

# Semi-Analytical Models for Lensing by Dark Halos: I. Splitting Angles

Li-Xin Li and Jeremiah P. Ostriker

*Princeton University Observatory, Princeton, NJ 08544-1001, USA*

E-mail: lxl, jpo@astro.princeton.edu

## ABSTRACT

We use the semi-analytical approach to analyze gravitational lensing of remote quasars by foreground dark halos in various cold dark matter (CDM) cosmologies, in order to determine the sensitivity of the predictions for probabilities of images separations to the input assumptions regarding the properties of halos and cosmological models. The power spectrum of primordial fluctuations is normalized by the cluster abundance constraints. The mass function of dark halos is assumed to be given by the Press-Schechter function. The mass density profile of dark halos is alternatively taken to be the singular isothermal sphere (SIS), the Navarro-Frenk-White (NFW) profile, or the generalized NFW profile. The cosmologies being considered include: the Einstein-de Sitter model (SCDM), the open model (OCDM), and the flat  $\Lambda$ -model (LCDM). As expected, we find that the lensing probability is extremely sensitive to the mass density profile of lenses (dark halos), and somewhat less so to the mean mass density in the universe, and the amplitude of primordial fluctuations. NFW halos are very much less effective in producing multiple images than SIS halos. For NFW lenses, the SCDM model produces lensing events fewer than the OCDM/LCDM models by two orders of magnitude. For SIS lenses, the SCDM model produces more lensing events with small splitting angles but produces fewer lensing events with large splitting angles than the OCDM/LCDM models, which is due to the fact that for large mass halos the Press-Schechter function is very sensitive to the amplitude of primordial fluctuations. In all cases the difference between the OCDM model and the LCDM model is not dramatic. None of these models can completely explain the current observations: the SIS models predict too many large splitting lenses, while the NFW models predict too few small splitting lenses. Essentially, the observed high ratio of small splitting to large splitting lenses is not predicted correctly. This indicates that there must be at least two populations of halos in the universe: small mass halos with a steep inner density slope and large mass

halos with a shallow inner density slope. A combination of SIS and NFW halos can reasonably reproduce the current observations, if we choose the mass for the transition from SIS to NFW to be  $\sim 10^{13}$  solar masses as might plausibly occur due to baryonic cooling and contraction in lower mass systems. Additionally, there is a tendency for CDM models to have too much power on small scales, i.e. too much mass concentration. From our sensitivity studies it appears that the cures proposed for other apparent difficulties of CDM would help here as well, an example being the warm dark matter (WDM) variant which is shown to produce large splitting lenses fewer than the corresponding CDM model by one order of magnitude.

*Subject headings:* cosmology: gravitational lensing — galaxies: clusters: general — galaxies: halos

## 1. Introduction

Gravitational lensing directly probes the mass distribution in the universe, so the investigation of lensing events of quasars at high redshifts can provide us with important information about cosmology and the matter distribution in the universe. A number of groups have attempted to test cosmological models by comparing lensing probabilities predicted by various cosmological models with those obtained from observations (Turner, Ostriker, & Gott 1984; Narayan & White 1988; Cen et al. 1994; Wambsganss et al. 1995; Maoz et al. 1997; Wambsganss, Cen, & Ostriker 1998; Bartelmann et al. 1998; Mortlock & Webster 2000; Porciani & Madau 2000; Keeton & Madau 2001). In the statistical study of cosmological gravitational lensing, two different approaches are used: one is to study the lensing probability of splitting angles of multiple images (Turner, Ostriker, & Gott 1984; Narayan & White 1988; Cen et al. 1994; Kochanek 1995; Wambsganss et al. 1995; Wambsganss, Cen, & Ostriker 1998; Porciani & Madau 2000; Keeton & Madau 2001), the other is to study the lensing probability of the length-to-width ratio of arcs formed by gravitational lensing (Bartelmann & Weiss 1994; Bartelmann et al. 1998; Cooray 1999; Kaufmann & Straumann 2000; Meneghetti et al. 2000). The two approaches reflect two different aspects of gravitational lensing and are complimentary to each other, both of them are directly related to observations and deserve detailed investigations. In this paper we focus on the splitting angles of multiple images caused by gravitational lensing. The case of length-to-width ratio of arcs will be considered in another paper. Results of the work done in testing cosmological scenarios to date are inconclusive with no clear preference found for any of the current models, and, overall, one could conclude that none of the studied models provides a good

fit to the rapidly improving observations. Perhaps the reason for this indeterminacy is that lensing also probes small scale structure. While this is known, its importance has perhaps not been appreciated sufficiently. Gravitational lensing provides an exquisitely sensitive test to the high frequency part of the power spectrum, because it is this part which establishes the central profiles of dark matter structures. Since lensing is comparably sensitive to input assumptions concerning the properties of lenses and of cosmological models, it is hazardous to use observed lensing statistics to draw inferences with regard to cosmology before determining the sensitivity to other factors. The primary purpose of this paper is to quantitatively assess the sensitivity of lensing expectations to the various input parameters so that this tool can be used to greatest effect.

To determine the probability for gravitational lensing, we need to know the mass density profile of lenses (dark halos), the mass function of lenses (which gives the number distribution of lenses over masses), the structure and global features of the universe (the universe is flat, closed, or open; the matter contents in the universe, etc), and the positions and shapes of the source objects (quasars). For studying the splitting angles of multiple images, it is enough to assume the source objects are points at high redshifts. In the framework of the Friedmann-Robertson-Walker models, there are a number of cosmologies as candidates for describing our universe, among which the most popular ones are the Einstein-de Sitter universe, which assumes a zero curvature and a zero cosmological constant; the open universe, which assumes a negative curvature and a zero cosmological constant; and the flat  $\Lambda$ -universe, which assumes a zero curvature and a positive cosmological constant (Peebles 1993; Ostriker & Steinhardt 1995). The matter contents in the universe are usually assumed to be dominated by dark matter: cold dark matter, warm or hot dark matter, or the mixture of them (Kolb & Turner 1990; Peebles 1993). Different kinds of dark matter give rise to different mass density profiles for dark halos. If the matter contents in the universe are dominated by cold dark matter (CDM), the three cosmological models are denoted respectively as SCDM (standard CDM = Einstein-de Sitter + CDM), OCDM (open + CDM), and LCDM (cosmological constant  $\Lambda$  + CDM).

The primordial fluctuations determine the mass distribution and the number density of dark halos in the universe. In studying gravitational lensing, the cosmological models, the matter contents in them, the power spectrum of the primordial fluctuations, and the source object positions are pre-assumed. Then the mass density fluctuations evolve according to the Einstein equations, which can be traced with numerical simulations. As time goes on, gravitationally bound objects (dark halos) are formed, which play the role of lenses. The mass density profile, and the mass function of dark halos in the universe are automatically derived from numerical simulations. Then, tracing the trajectories of light rays, we can obtain the number of lensing events and thus the lensing probability. This is the basic

spirit of numerical simulations for gravitational lensing (Wambsganss et al. 1995). With this approach, the mass density profile of lenses and the mass function of lenses appear as the results of simulations, they do not need to be pre-assumed. However, numerical simulations have their own limitations. First, numerical simulations usually take a great deal of computer time, which makes it inconvenient to test several different models at a time. Second, in every numerical simulation there are two limits on the spatial scales: the size of box, which is the maximum scale and determines the presence or absence of intrinsically rare events, and the size of fundamental cell (i.e. the resolution), which is the minimum scale. Correspondingly this gives rise the upper and lower bonds on the masses of halos formed in the simulation, which causes the result that the number of lensing events with small splitting angles (caused by halos with small masses) and large splitting angles (caused by rare halos with large masses) are underestimated. This last deficit is seen by comparing the simulation results of Wambsganss et al. (1995) with the analytical results of Kochanek (1995), which will also be confirmed by the results in this paper. Furthermore, the lensing cross-sections are very sensitive to inner most parts of the density profiles which are most subject to problems of numerical resolution (Ghigna et al. 2000; Klypin 2000). Ultimately, numerical simulations are required to best determine the expected halo properties. The current generation of numerical simulations has insufficient dynamical range to simultaneously address accurately both large and small scale structures, but forthcoming  $1024^3$ -particle simulations may remedy this defect. For the present, semi-analytical methods may be best adapted to explore the sensitivity of the results to the input parameters.

In the semi-analytical approach, the mass density profile and the mass function of lenses are pre-assumed and can be adjusted to fit various dark matter scenarios. Though this makes us rely on an assumed density profile and mass function, it has the advantage that the calculation of the lensing probability can be handled with semi-analytical methods, which takes much less computer time than numerical simulations, so several different models can easily be tested at a time. And, in this approach, there are not the limitations in spatial scales and mass scales necessitated by numerical simulations; the lensing probability for small splitting angles and large splitting angles can be obtained accurately for any assumed halo density profile, the most critical feature of which is the steepness of the central density profile which may be parameterized by the central slope,  $-\alpha$ . The mass density profile is often taken to be the singular isothermal sphere (SIS,  $\alpha = 2$ ) (Gott & Gunn 1974); the mass function is usually taken to be the Press-Schechter function (Press & Schechter 1974). Though the SIS profile is simple, it does not fit the CDM simulation results well. Navarro, Frenk, & White (1996, 1997) have proposed a “universal” density profile (the so-called NFW profile,  $\alpha = 1$ ) which has been shown to fit the simulation results better. A generalized NFW (GNFW) profile with somewhat steeper inner slopes intermediate between NFW and

SIS appears to provide a still better fit to simulated profiles (Zhao 1996; Subramanian, Cen, & Ostriker 2000; Ghigna et al. 2000; Jing & Suto 2000; Wyithe, Turner, & Spergel 2000) for which typically  $\alpha = 1.4 \pm 0.1$ . With N-body simulations of the SCDM scenario (Efstathiou 1990; Kauffmann & White 1993), or comparison with observations (Bahcall & Cen 1993; Girardi et al. 1998; Girardi & Giuricin 2000), the Press-Schechter mass function has been shown to describe the mass distribution in the universe quite accurately.

In this paper we use the semi-analytical approach to investigate the gravitational lensing of quasars by foreground dark halos. We work with three kinds of cosmological models: SCDM, OCDM, and LCDM models. The mass function of dark halos is taken to be the Press-Schechter function. The power spectrum of primordial fluctuations is normalized by the cluster abundance constraints (Wang & Steinhardt 1998; Wang et al. 2000). We alternatively consider three kinds of density profiles: SIS, NFW, and GFW profiles, where the last model allows us to estimate (by varying the free parameters in the GFW profile) variants of the CDM scenario. For the various models we will calculate the lensing probability of splitting angles of multiple images, and test the sensitivity of the lensing probability to the input parameters regarding the properties of halos and cosmological models.

The paper is organized as follows: In section 2 we outline the cosmological models to be calculated in the paper, and introduce the power spectrum of primordial fluctuations and the Press-Schechter function. In section 3 the most simple case is investigated – SIS halos as lenses. We find that, the SCDM model produces fewer lensing events with large splitting angles, but more lensing events with small splitting angles than the OCDM model and the LCDM model. This is due to the fact that for large splitting angles, which are produced by large mass halos, the Press-Schechter function is exponentially sensitive to the amplitude of primordial fluctuations and the SCDM model has the smallest amplitude of primordial fluctuations; but for small splitting angles, which are produced by small mass halos, the Press-Schechter function is not sensitive to the amplitude of primordial fluctuations but the mean mass density in the universe plays a more dominant role. In section 4 we consider the case for the NFW profile and the GFW profile. As expected, we find that, the lensing probability is very sensitive to the mass density profile of the lenses. The more concentrated toward center the density distribution is, the higher lensing probability it produces. Compared to a SIS halo, a NFW halo is very ineffective in producing multiple images. For the NFW profile, the SCDM model produces the least lensing events: the OCDM model and the LCDM model produce a comparable number of lensing events which exceed the number of lensing events produced by the SCDM model by two orders of magnitudes. This is mainly due to two facts: a NFW model in a SCDM universe has the smallest concentration parameter, and a SCDM universe has the smallest amplitude of fluctuations. In section 5, we compare our predictions with observations. We find that, none of the models can ex-

plain the current observations: the SIS models predict too many lensing events with large splitting angles, while the NFW models predict too few lensing events with small splitting angles. Essentially, the observed high ratio of small splitting to large splitting events is not predicted correctly. By a combination of them – using the SIS profile for small mass halos and the NFW profile for large mass halos, we show that the observation results can be reasonably re-produced if we choose the mass at the transition point between the two halo populations to be  $\sim 10^{13}$  solar masses – the mass of halos below which cooling of the corresponding baryonic component will lead to concentration of the baryons to the inner parts of the mass profile (Rees & Ostriker 1977; Blumenthal et al. 1986; Porciani & Madau 2000). Our results indicate that the halos in the universe cannot be described by a single universal density profile, there exist at least two halo populations: small mass halos with a steep inner density slope (the inner parts dominated by the baryonic component), and large mass halos with a shallow inner density slope (within which baryons and dark matter have essentially the same profiles). In section 6, we draw our conclusions.

The failure of the SIS, and GNFW ( $\alpha = 1.5$ ) models at large splitting angles appears to be another manifestation of the tendency for CDM models to have too much power on small scales, i.e. too much mass concentration. From our sensitivity studies it appears that the cures proposed for other difficulties of CDM would help here as well, an example being the warm dark matter (WDM) variant, for which  $\alpha$  tends to be smaller (Bode, Ostriker, & Turok 2000). A model very roughly designed to match a WDM variant has a greatly reduced probability of large splitting angles: lower than the corresponding probability for the CDM model by one order of magnitude.

## 2. Cosmological Models

The lensing probability is basically determined by three factors: (1) the positions of source objects; (2) the positions, the density profile, and the mass function of lenses; (3) the cosmological model. In this section we define the cosmological models that will be studied in this paper, and introduce the mass function of dark halos.

### 2.1. Cosmological functions

The cosmological models are classified with parameters  $\Omega_m$ ,  $\Omega_\Lambda$ , and  $\Omega_R$ , which are respectively defined by (Peebles 1993)

$$\Omega_m \equiv \frac{\rho_0}{\rho_{\text{crit},0}}, \quad \Omega_\Lambda \equiv \frac{\Lambda}{8\pi G \rho_{\text{crit},0}}, \quad \Omega_R \equiv \frac{-3k}{8\pi G \rho_{\text{crit},0} a_0^2}, \quad (1)$$

where  $\rho_0$  is today's average mass density (dark matter + baryonic matter + radiation) in the universe,  $G$  is the gravitational constant,  $\Lambda$  is the cosmological constant,  $a_0$  is today's scale of the universe,  $k = 0, \pm 1$  is the spatial curvature of the universe,  $\rho_{\text{crit},0}$  is today's critical mass density of the universe which is defined by

$$\rho_{\text{crit},0} \equiv \frac{3H_0^2}{8\pi G} \approx 1.88 \times 10^{-29} h^2 \text{ g cm}^{-3}, \quad (2)$$

where  $H_0 = 100h \text{ km s}^{-1} \text{ Mpc}^{-1}$  is the Hubble constant. The Einstein equations tell us that  $\Omega_m + \Omega_\Lambda + \Omega_R = 1$ . Thus, among  $\Omega_m$ ,  $\Omega_\Lambda$ , and  $\Omega_R$ , only two of them are independent parameters. In this paper we assume that the matter in the universe is dominated by cold dark matter (CDM), and we consider three kinds of universes:

1. *Einstein-de Sitter model* (SCDM). In this model,  $\Omega_m = 1$ ,  $\Omega_\Lambda = \Omega_R = 0$ , and  $k = 0$ . The linear growth function, which describes the growth speed of the linear perturbation in the universe (Peebles 1980), is

$$\mathcal{D}(z) = \frac{1}{1+z}, \quad (3)$$

where  $z$  is the cosmic redshift. The linear growth function is normalized to be unity at present epoch:  $\mathcal{D}(z=0) = 1$ .

2. *Open model* (OCDM). In an open universe,  $0 < \Omega_m < 1$ ,  $\Omega_\Lambda = 0$ ,  $0 < \Omega_R = 1 - \Omega_m < 1$ , and  $k = -1$ . The linear growth function is

$$\mathcal{D}(z) = \frac{F_1\left(\frac{\Omega_m^{-1}-1}{1+z}\right)}{F_1(\Omega_m^{-1}-1)}, \quad (4)$$

where

$$F_1(x) \equiv 1 + \frac{3}{x} + \frac{3(1+x)^{1/2}}{x^{3/2}} \ln [(1+x)^{1/2} - x^{1/2}]. \quad (5)$$

$F_1$  is fitted by

$$F_1(x) \approx 1 - \left(\frac{1.5}{x+1.5}\right)^{0.6} \quad (6)$$

with an error  $< 1.3\%$  for  $10^{-5} < x < 10$ .

3.  $\Lambda$ -*model* (LCDM). A  $\Lambda$ -universe has  $0 < \Omega_m < 1$ ,  $0 < \Omega_\Lambda = 1 - \Omega_m < 1$ ,  $\Omega_R = 0$ , and  $k = 0$ . The linear growth function is

$$\mathcal{D}(z) = \frac{F_2\left[\frac{(2\Omega_\Lambda/\Omega_m)^{1/3}}{1+z}\right]}{F_2[(2\Omega_\Lambda/\Omega_m)^{1/3}]}, \quad (7)$$

where

$$F_2(x) \equiv \left( \frac{x^3 + 2}{x^3} \right)^{1/2} \int_0^x \left( \frac{u}{u^3 + 2} \right)^{3/2} du. \quad (8)$$

$F_2$  is fitted by

$$F_2(x) \approx 0.358 \left[ 1 - (1 + 0.23 x^{2.2})^{-1.26} \right]^{1/2.2} \quad (9)$$

with an error  $< 2\%$  for  $0 < x < 10^4$ .

For all the three cosmological models, the proper cosmological distance from an object at redshift  $z_1$  to an object at redshift  $z_2$  along the same line of sight is (Peebles 1993)

$$D(z_1, z_2) = \frac{c}{H_0} \int_{z_1}^{z_2} \frac{(1+z)^{-1} dz}{\sqrt{\Omega_m(1+z)^3 + \Omega_R(1+z)^2 + \Omega_\Lambda}}, \quad (10)$$

where  $c$  is the speed of light. In studying gravitational lensing, another useful distance is the angular-diameter distance. The angular-diameter distance from an object at redshift  $z_1$  to an object at redshift  $z_2$  along the same line of sight is (Bartelmann & Schneider 2001)

$$D^A(z_1, z_2) = \frac{c/H_0}{1+z_2} \begin{cases} |\Omega_R|^{-1/2} \sin \left[ |\Omega_R|^{1/2} w \right] & (k=1), \\ w & (k=0), \\ \Omega_R^{-1/2} \sinh \left[ \Omega_R^{1/2} w \right] & (k=-1), \end{cases} \quad (11)$$

where

$$w(z_1, z_2) \equiv \int_{z_1}^{z_2} \frac{dz}{\sqrt{\Omega_m(1+z)^3 + \Omega_R(1+z)^2 + \Omega_\Lambda}}. \quad (12)$$

Note that  $D(z_1, z_2) = D(z_2, z_1)$  and  $D(z_1, z_2) = D(0, z_2) - D(0, z_1)$ , but  $D^A(z_1, z_2) \neq D^A(z_2, z_1)$  and  $D^A(z_1, z_2) \neq D^A(0, z_2) - D^A(0, z_1)$ . But we have

$$(1+z_2) D^A(z_1, z_2) = (1+z_1) D^A(z_2, z_1). \quad (13)$$

## 2.2. Mass fluctuations

Dark halos of galaxies and galaxy clusters are formed from primordial fluctuations of matter in the early universe. For a fluctuation with a power spectrum  $P_k = |\delta_k|^2$ , its variance on a scale of comoving radius  $r$  is (Kolb & Turner 1990)

$$\Delta^2(r) \equiv \left( \frac{\delta M}{M} \right)^2 = (2\pi)^{-3} \int_0^\infty 4\pi k^2 dk P_k W^2(kr), \quad (14)$$



where  $W(kr)$  is the Fourier transformation of a window function. For a top-hat window function

$$W(kr) = 3 \left[ \frac{\sin kr}{(kr)^3} - \frac{\cos kr}{(kr)^2} \right], \quad (15)$$

for a Gaussian window function

$$W(kr) = \exp[-k^2 r^2/2]. \quad (16)$$

In this paper we use the top-hat window function. We compute the CDM power spectrum using the fitting formulae given by Eisenstein & Hu (1999)

$$\frac{k^3}{2\pi^2} P(k, z) = \delta_H^2 \left( \frac{ck}{H_0} \right)^{3+n} T^2(k) \mathcal{D}(z)^2, \quad (17)$$

where  $\delta_H$  is the amplitude of perturbations on the horizon scale today,  $n$  is the initial power spectrum index,  $\mathcal{D}(z)$  is the linear growth function, and

$$T = \frac{L}{L + Cq_{eff}^2}, \quad (18)$$

where

$$L \equiv \ln(e + 1.84q_{eff}), \quad q_{eff} \equiv \frac{k}{\Omega_m h^2 \text{Mpc}^{-1}}, \quad (19)$$

$$C \equiv 14.4 + \frac{325}{1 + 60.5q_{eff}^{1.11}}. \quad (20)$$

We normalize the power spectrum to  $\sigma_8^2 \equiv \Delta^2(z=0, r=8h^{-1}\text{Mpc})$ , then

$$\delta_H = \frac{\sigma_8}{\left[ \int_0^\infty \frac{dk}{k} \left( \frac{ck}{H_0} \right)^{3+n} T^2(k) W^2(kr_8) \right]^{1/2}}. \quad (21)$$

The value of  $\sigma_8$  can be estimated from the cluster abundance constraints (Wang & Steinhardt 1998; Wang et al. 2000)

$$\sigma_8 \Omega_m^\gamma \approx 0.5, \quad (22)$$

where  $\gamma \approx 0.43 + 0.33\Omega_m$  for LCDM and  $\gamma \approx 0.33 + 0.35\Omega_m$  for OCDM. For a scale-invariant spectrum predicted by the inflation theory and being consistent with observed cosmic microwave background (CMB) fluctuations, we have  $n = 1$  (Kolb & Turner 1990).

### 2.3. Mass function of dark halos

Assume the primordial density fluctuations are Gaussian. Then, according to the Press-Schechter theory (Press & Schechter 1974), the comoving number density of dark halos formed by redshift  $z$  with mass in the range  $(M, M + dM)$  is

$$n(M, z) dM = \frac{\rho_0}{M} f(M, z) dM, \quad (23)$$

where  $\rho_0 \equiv \Omega_m \rho_{\text{crit},0}$  is the present mean mass density in the universe,  $f(M, z)$  is the Press-Schechter function

$$f(M, z) = -\sqrt{\frac{2}{\pi}} \frac{\delta_c(z)}{M\Delta} \frac{d \ln \Delta}{d \ln M} \exp \left[ -\frac{\delta_c^2(z)}{2\Delta^2} \right], \quad (24)$$

where  $\Delta^2 = \Delta^2(M, z = 0)$  is the present variance of the fluctuations in a sphere containing a mean mass  $M$ , and  $\delta_c(z)$  is the density threshold for spherical collapse by redshift  $z$ . The redshift-dependent density threshold has been calculated by many people (Lacey & Cole 1993; Kochanek 1995; Eke, Cole, & Frenk 1996, and references therein), here we use the approximation (Navarro, Frenk, & White 1997)

$$\delta_c(z) = \frac{\delta_c^0[\Omega(z)]}{\mathcal{D}(z)}, \quad (25)$$

where

$$\Omega(z) \equiv \frac{\rho}{\rho_{\text{crit}}} = \frac{\Omega_m(1+z)^3}{\Omega_m(1+z)^3 + \Omega_R(1+z)^2 + \Omega_\Lambda}, \quad (26)$$

$\mathcal{D}(z)$  is the linear growth function normalized to unity at  $z = 0$ , and

$$\delta_c^0(\Omega) \approx 1.6865 \times \begin{cases} 1, & \text{if } \Omega_m = 1 \text{ and } \Lambda = 0 \\ \Omega^{0.0185}, & \text{if } \Omega_m < 1 \text{ and } \Lambda = 0 \\ \Omega^{0.0055}, & \text{if } \Omega_m + \Omega_\Lambda = 1 \end{cases}. \quad (27)$$

To a very good approximation  $\delta_c(z)\mathcal{D}(z) \approx 1.69$  for all cosmological models with  $\Omega_m > 0.1$ .

In equation (24),  $r$  is related to  $M$  by

$$M = \frac{4\pi}{3} \rho_0 r^3 = \frac{4\pi}{3} \Omega_m \rho_{\text{crit},0} r^3, \quad (28)$$

i.e.

$$r = 9.510 \left( \frac{1}{\Omega_m} \frac{M}{10^{15} h^{-1} M_\odot} \right)^{1/3} h^{-1} \text{Mpc}. \quad (29)$$

Though it is obtained from very simple considerations, the Press-Schechter function has been shown to be in remarkable agreement with N-body simulations for the standard cold dark matter scenario (Efstathiou 1990; Kauffmann & White 1993) and observations (Bahcall & Cen 1993; Girardi et al. 1998; Girardi & Giuricin 2000).

The fluctuation variance  $\Delta^2$  decreases with increasing mass  $M$ . Thus, from equation (24),  $f(M, z)$  decreases exponentially with increasing  $M$ . Because of this, a crude knowledge of  $f(M, z)$  at the large mass end gives a strict constraint on cosmological parameters (Chiu, Ostriker, & Strauss 1998). To see this, let us write the Press-Schechter function in the form

$$f(M, z, \sigma_8) = \frac{f_1(M, z)}{\sigma_8} \exp \left[ -\frac{A(M, z)}{\sigma_8^2} \right], \quad (30)$$

where we have used the fact that  $\Delta \propto \sigma_8$ . From equation (30), we have

$$\frac{\delta f}{f} = \frac{\delta \sigma_8}{\sigma_8} \left( \frac{2A}{\sigma_8^2} - 1 \right). \quad (31)$$

So, if  $A/\sigma_8^2 \gg 1/2$  – which is true for large  $M$  – a large error in  $f$  corresponds to a small error in  $\sigma_8$ . As a simple example, consider a power law spectrum  $P_k \propto k^{n_1}$ , then we have

$$\Delta^2(M) = \sigma_8^2 \left[ 1.189 \left( \frac{1}{\Omega_m} \frac{M}{10^{15} h^{-1} M_\odot} \right)^{1/3} \right]^{-n_1-3}, \quad (32)$$

and

$$\frac{2A}{\sigma_8^2} \propto M^{\frac{n_1+3}{3}} D(z)^{-2} \sigma_8^{-2}. \quad (33)$$

For large  $M$  and large  $z$ , a large  $\delta f/f$  corresponds to a small  $\delta \sigma_8/\sigma_8$  if  $n_1 > -3$ .

In the upper panel of Fig. 1 we plot the Press-Schechter function  $f$  against the velocity dispersion  $\sigma_v$  of dark halos at  $z = 0$  in a SCDM cosmology, where the CDM power spectrum is given by equation (17). The velocity dispersion of a dark halo is defined by

$$\sigma_v \equiv \left( \frac{GM}{2r_{200}} \right)^{1/2}, \quad (34)$$

where  $r_{200}$  is the radius of a sphere around a dark halo within which the average mass density is 200 times the critical mean mass density of the universe, i.e.

$$\frac{M}{\frac{4\pi}{3} r_{200}^3} = 200 \rho_{\text{crit}}, \quad (35)$$

and  $M \equiv M_{200}$  is the mass within that sphere

$$M \equiv M_{200} = 4\pi \int_0^{r_{200}} \rho r^2 dr. \quad (36)$$

From equation (34) and equation (35), we have

$$\begin{aligned} M &= \frac{\sigma_v^3}{G} \left( \frac{3}{100\pi G \rho_{\text{crit}}} \right)^{1/2} \\ &= 0.656 \times 10^{15} h^{-1} M_{\odot} \sigma_{v,1000}^3 [\Omega_m(1+z)^3 + \Omega_R(1+z)^2 + \Omega_{\Lambda}]^{-1/2}, \end{aligned} \quad (37)$$

where  $M_{\odot}$  is the solar mass,  $\sigma_{v,1000} \equiv \frac{\sigma_v}{1000 \text{ km/s}}$ , and we have used

$$\rho_{\text{crit}}(z) = \rho_{\text{crit},0} \frac{\Omega_m}{\Omega(z)} (1+z)^3 = \rho_{\text{crit},0} [\Omega_m(1+z)^3 + \Omega_R(1+z)^2 + \Omega_{\Lambda}]. \quad (38)$$

In the upper panel of Fig. 1, the solid curve is for the case of  $\sigma_8 = 0.5$ , the dashed curve is for the case of  $\sigma_8 = 0.6$ . It clearly shows that with the same amount of change in  $\sigma_8$ , a larger change in  $f$  happens at the end of large  $\sigma_v$ . In the lower panel of Fig. 1, we plot  $\zeta \equiv \frac{\delta f/f}{\delta \sigma_8/\sigma_8}$  against  $\sigma_v$  for a SCDM cosmology with  $z = 0$  and  $\sigma_8 = 0.5$ . Again, it shows that for large  $\sigma_v$  a poor knowledge in  $f$  gives a good estimation of  $\sigma_8$ . This is true because the number density of halos with high velocity dispersion (which is true for rich clusters of galaxies) is very sensitive to the value of  $\sigma_8$ . Thus, since lensing is produced primarily by the highest velocity dispersion clusters, the observed number of lenses will sensitively constrain the value of  $\sigma_8$ .

### 3. Lensing by a Singular Isothermal Sphere

#### 3.1. Singular isothermal sphere as a lens

The most simple model for a lens is a singular isothermal sphere (SIS) with a mass density

$$\rho(r) = \frac{\sigma_v^2}{2\pi G} \frac{1}{r^2}, \quad (39)$$

where  $\sigma_v$  is the velocity dispersion (Gott & Gunn 1974; Turner, Ostriker, & Gott 1984; Schneider, Ehlers, & Falco 1992). Though it is simple, this model can describe the flat rotation curves of galaxies and many basic features of gravitational lensing. Though the gravitational lensing by a SIS has been well studied in the literature (Gott & Gunn 1974; Turner, Ostriker, & Gott 1984; Narayan & White 1988; Kochanek 1995), we present it here

since we are using an updated CDM power spectrum and we want to compare its results with those for the NFW and the GFW cases.

The surface mass density of the SIS is

$$\Sigma(\xi) = \frac{\sigma_v^2}{2G} \frac{1}{\xi}, \quad (40)$$

where  $\xi \equiv |\vec{\xi}|$ ,  $\vec{\xi}$  is the position vector in the lens plane. Choose the length scales in the lens plane and the source plane to be respectively

$$\xi_0 = 4\pi \left(\frac{\sigma_v}{c}\right)^2 \frac{D_L^A D_{LS}^A}{D_S^A}, \quad \eta_0 = \xi_0 \frac{D_S^A}{D_L^A}, \quad (41)$$

where  $D_S^A$  is the angular-diameter distance from the observer to the source object,  $D_L^A$  is the angular-diameter distance from the observer to the lens object,  $D_{LS}^A$  is the angular-diameter distance from the lens to the source object. Remember that  $D_{LS}^A \neq D_S^A - D_L^A$ . Then the position vector of a point in the lens plane can be written as  $\vec{\xi} = \vec{x}\xi_0$ , the position vector of a point in the source plane can be written as  $\vec{\eta} = \vec{y}\eta_0$ . The lensing equation is

$$y = x - \frac{m(x)}{x}, \quad (42)$$

where

$$m(x) \equiv 2 \int_0^x \frac{\Sigma(x')}{\Sigma_{\text{cr}}} x' dx', \quad (43)$$

where the critical surface mass density  $\Sigma_{\text{cr}}$ , defined by (Turner, Ostriker, & Gott 1984)

$$\Sigma_{\text{cr}} \equiv \frac{c^2}{4\pi G} \frac{D_S^A}{D_L^A D_{LS}^A}, \quad (44)$$

is of the order of the surface density of the universe.

Inserting equation (40) and equation (44) into equation (43), then into equation (42), we obtain  $\Sigma/\Sigma_{\text{cr}} = (2|x|)^{-1}$  and

$$y = x - \frac{|x|}{x}. \quad (45)$$

Double images are formed if and only if  $|y| \leq 1$ , i.e.  $|x| \leq 1$ . The separation between the two images is

$$\Delta x = 2, \quad (46)$$

thus the splitting angle is

$$\Delta\theta = \frac{\xi_0}{D_L^A} \Delta x = 8\pi \left(\frac{\sigma_v}{c}\right)^2 \frac{D_{LS}^A}{D_S^A} = 0.9613' \sigma_{v,1000}^2 \frac{D_{LS}^A}{D_S^A}. \quad (47)$$

Using equation (37), we have

$$\Delta\theta = \frac{8\pi}{c^2} \left(\frac{100\pi}{3} G^3 M^2 \rho_{\text{crit}}\right)^{1/3} \frac{D_{LS}^A}{D_S^A} = 1.271' \frac{D_{LS}^A}{D_S^A} \left(\frac{M}{10^{15} h^{-1} M_\odot}\right)^{2/3} \left(\frac{\rho_{\text{crit}}}{\rho_{\text{crit},0}}\right)^{1/3}. \quad (48)$$

The cross-section (defined in the lens plane) for forming two images with splitting angle  $\Delta\theta > \Delta\theta_0$  is

$$\sigma = \pi \xi_0^2 \vartheta(\Delta\theta - \Delta\theta_0) = \pi \xi_0^2 \vartheta(M - M_0), \quad (49)$$

where  $\vartheta$  is the step function

$$\vartheta(u - v) = \begin{cases} 1, & \text{if } u > v \\ 0, & \text{if } u < v \end{cases}, \quad (50)$$

and

$$\begin{aligned} M_0 &= \left(\frac{3}{100\pi}\right)^{1/2} \frac{c^3}{G^{3/2} \rho_{\text{crit}}^{1/2}} \left(\frac{\Delta\theta_0}{8\pi}\right)^{3/2} \left(\frac{D_S^A}{D_{LS}^A}\right)^{3/2} \\ &= 0.6975 \times 10^{15} h^{-1} M_\odot \left(\frac{\Delta\theta_0}{1'}\right)^{3/2} \left(\frac{D_S^A}{D_{LS}^A}\right)^{3/2} \left(\frac{\rho_{\text{crit}}}{\rho_{\text{crit},0}}\right)^{-1/2}. \end{aligned} \quad (51)$$

### 3.2. Lensing probability by a singular isothermal sphere

The integral lensing probability for a source object at redshift  $z_s$  is (Schneider, Ehlers, & Falco 1992)

$$P = \int_0^{z_s} \frac{dP}{dz} dz, \quad (52)$$

where  $z$  is the redshift of lenses, and

$$\begin{aligned} \frac{dP}{dz} &= \frac{dD_L}{dz} \int_0^\infty \bar{n}(M, z) \sigma(M, z) dM \\ &= \rho_{\text{crit},0} \Omega_m (1+z)^3 \frac{dD_L}{dz} \int_0^\infty \frac{1}{M} f(M, z) \sigma(M, z) dM, \end{aligned} \quad (53)$$

where  $\bar{n}(M, z)dM \equiv n(M, z)(1+z)^3dM$  is the physical number density of dark halos of masses between  $M$  and  $M+dM$ ,  $n(M, z)dM$  is the comoving number density of dark halos of masses between  $M$  and  $M+dM$ ,  $\sigma(M, z)$  is the lensing cross-section for a dark halo of mass  $M$  at redshift  $z$ ,  $f(M, z)$  is the mass function of dark halos. Here  $D_L$  is the proper distance from the observer to the lens object.

If we use  $10^{15}h^{-1}M_\odot$  as the unit of  $M$ , then the unit of  $f(M, z)$  is  $(10^{15}h^{-1}M_\odot)^{-1}$ . Define  $M_{15} \equiv M/(10^{15}h^{-1}M_\odot)$ . Let us use  $c/H_0 = 2997.9h^{-1}\text{Mpc}$  as the unit for cosmological distances, and  $h^{-1}\text{Mpc}$  as the unit for local lengths (thus the unit of  $\sigma$  is  $h^{-2}\text{Mpc}^2$ ), then

$$\frac{dP}{dz} = 0.8321 \Omega_m (1+z)^3 \frac{d}{dz} \left( \frac{D_L}{c/H_0} \right) \int_0^\infty f(M_{15}, z) \left[ \frac{\sigma(M_{15}, z)}{1h^{-2}\text{Mpc}^2} \right] \frac{dM_{15}}{M_{15}}. \quad (54)$$

Inserting equation (49) and equation (41) into equation (53), we have for the SIS case

$$\frac{d}{dz} P(> \Delta\theta_0) = 16\pi^3 \rho_{\text{crit},0} \Omega_m (1+z)^3 \frac{dD_L}{dz} \left( \frac{D_L^A D_{LS}^A}{D_S^A} \right)^2 \int_{M_0}^\infty \frac{1}{M} f(M, z) \left( \frac{\sigma_v}{c} \right)^4 dM, \quad (55)$$

where  $\sigma_v/c$  is related to  $M$  by the reverse of equation (37), i.e.

$$\begin{aligned} \frac{\sigma_v}{c} &= \left( \frac{M}{M_1} \right)^{1/3} \left[ \Omega_m (1+z)^3 + \Omega_R (1+z)^2 + \Omega_\Lambda \right]^{1/6} \\ &= 3.836 \times 10^{-3} M_{15}^{1/3} \left[ \Omega_m (1+z)^3 + \Omega_R (1+z)^2 + \Omega_\Lambda \right]^{1/6}, \end{aligned} \quad (56)$$

where

$$M_1 \equiv \left( \frac{3c^6}{100\pi G^3 \rho_{\text{crit},0}} \right)^{1/2} = 1.772 \times 10^{22} h^{-1} M_\odot. \quad (57)$$

Or, from equations (49), (41), and (54), we have

$$\begin{aligned} \frac{d}{dz} P(> \Delta\theta_0) &= 0.4593 \Omega_m (1+z)^3 \left( \frac{D_R^A}{c/H_0} \right)^2 \frac{d}{dz} \left( \frac{D_L}{c/H_0} \right) \\ &\quad \times \int_{M_0}^\infty f(M_{15}, z) \left( \frac{\sigma_v}{10^3 \text{km/s}} \right)^4 \frac{dM_{15}}{M_{15}}, \end{aligned} \quad (58)$$

where  $D_R^A \equiv D_L^A D_{LS}^A / D_S^A$ .

With equations (52), (56), and (58), we can calculate  $dP(> \Delta\theta_0)/dz$  and  $P(> \Delta\theta_0)$  for a given cosmology (specified by  $\Omega_m$ ,  $\Omega_\Lambda$ , and the Hubble constant  $h$ ), a given primary perturbation (specified by  $\sigma_8$ ), and a given position of the source object ( $z_s$ ), assuming the CDM power spectrum is given by equation (17) and the mass function of dark halos is given

by equation (24). In our numerical calculations we assume  $h = 0.7$ ,  $z_s = 1.5$ , and  $\sigma_8$  is related to  $\Omega_m$  by equation (22). In Fig. 2 and Fig. 3 we show the results for three typical cosmological models: SCDM with  $\Omega_m = 1$  and  $\sigma_8 = 0.5$ ; OCDM with  $\Omega_m = 0.3$ ,  $\Omega_\Lambda = 0$ , and  $\sigma_8 = 0.85$ ; and LCDM with  $\Omega_m = 0.3$ ,  $\Omega_\Lambda = 0.7$ , and  $\sigma_8 = 0.95$ .

Fig. 2 shows the differential lensing probability  $dP/dz$  for  $\Delta\theta > \Delta\theta_0 = 5''$ . The maximum of  $dP/dz$  is at  $z \approx 0.3$  for SCDM, at  $z \approx 0.4$  for OCDM and LCDM. Median expected redshifts for the three models are respectively 0.349, 0.455, and 0.461. This is consistent with the demonstration that the differential lensing probability peaks at intermediate redshifts (i.e. roughly the half way to the source object; Turner, Ostriker, & Gott 1984) and with the scenario that structures form later in the SCDM model than in OCDM and LCDM models (Longair 1998; Bartelmann et al. 1998). As is well known structure forms earlier in low  $\Omega_m$  universes, so the relative probability of a lens being at  $z = 0.1$  rather than 1.0 is orders of magnitude higher in SCDM than it is in OCDM/LCDM. Fig. 3 shows the integral probability  $P(> \Delta\theta)$  as a function of the splitting angle  $\Delta\theta$ . For small  $\Delta\theta$ , the SCDM model produces more lensing events than the OCDM and the LCDM models, which is a manifestation of the fact that the SCDM universe has a higher mean mass density than the OCDM and the LCDM universes. For large  $\Delta\theta$ , the SCDM model produces less lensing events than the OCDM and the LCDM models, which is caused by the fact that at large mass end the Press-Schechter function is very sensitive to  $\sigma_8$  (see Fig. 1) while the SCDM model has a much smaller  $\sigma_8$  than the OCDM and the LCDM models. The difference in the lensing probabilities for the OCDM model and the LCDM model is mainly due to the effect of the cosmological constant: the cosmological constant tends to increase the lensing probability (Turner 1990), primarily because there is a greater metric distance and thus more potential lenses between an observer and a source with a given redshift in  $\Lambda$  cosmologies.

## 4. Lensing by a Generalized NFW Model

### 4.1. The generalized NFW model as a lens

The SIS model is simple and can describe many observational features of galaxies and galaxy clusters. However, the SIS does not fit well the density profiles predicted by N-body numerical simulations (Frenk et al. 1985, 1988; Quinn, Salmon, & Zurek 1986; Efsthathiou et al. 1988; Zurek, Quinn, & Salmon 1988; Warren et al. 1992; Crone, Evrard, & Richstone 1994). Navarro, Frenk, & White (1996, 1997) proposed a “universal” mass density profile for dark halos: the so-called NFW profile, which fits the simulation results better than the



SIS. The NFW profile is

$$\rho_{\text{NFW}}(r) = \frac{\rho_s r_s^3}{r(r + r_s)^2}, \quad (59)$$

where  $\rho_s$  and  $r_s$  are constants. At large radii ( $r \gg r_s$ )  $\rho_{\text{NFW}} \sim r^{-3}$ , at small radii ( $r \ll r_s$ )  $\rho_{\text{NFW}} \sim r^{-1}$ , both are different from the SIS. At intermediate radii the NFW profile resembles the SIS. Though Navarro, Frenk, & White demonstrated that over two decades in radius their profile accurately fits halos with mass spanning about four orders of magnitude ranging from dwarf galaxy halos to those of rich galaxy clusters, with higher resolution simulations Jing & Suto (2000) have argued that the NFW profile is not correct on small scales. Furthermore, Subramanian, Cen, & Ostriker (2000) and Ghigna et al. (2000) have emphasized the dependence of the inner slope of halo mass density on the form of the power spectrum of the primordial fluctuations. Therefore, here we consider a generalized NFW (GNFW) profile (Zhao 1996)

$$\rho(r) = \frac{\rho_s r_s^3}{r^\alpha (r + r_s)^{3-\alpha}}, \quad (60)$$

where  $\alpha$  ( $0 < \alpha < 3$ ) is a new constant parameter. The NFW profile is a specific case of the GNFW profile when  $\alpha = 1$ . Obviously, at large radii ( $r \gg r_s$ ) the GNFW profile has the same behavior as the NFW profile. But on small scales ( $r \ll r_s$ ) they are different unless  $\alpha = 1$ . When  $\alpha = 2$ , the GNFW profile resembles an SIS on small scales but resembles the NFW profile on large scales.

The surface mass density for the GNFW profile is

$$\Sigma(x) = 2\rho_s r_s \int_0^\infty (x^2 + z^2)^{-\alpha/2} \left[ (x^2 + z^2)^{1/2} + 1 \right]^{-3+\alpha} dz, \quad (61)$$

where  $x = |\vec{x}|$  and  $\vec{x} = \vec{\xi}/r_s$ ,  $\vec{\xi}$  is the position vector in the lens plane. Inserting equation (61) into equation (42) and equation (43), we obtain the lensing equation for a GNFW halo

$$y = x - \mu_s \frac{g(x)}{x}, \quad (62)$$

where  $y = |\vec{y}|$ ,  $\vec{\eta} = \vec{y} r_s D_S^A / D_L^A$  is the position vector in the source plane, and

$$g(x) \equiv \int_0^x u du \int_0^\infty (u^2 + z^2)^{-\alpha/2} \left[ (u^2 + z^2)^{1/2} + 1 \right]^{-3+\alpha} dz, \quad (63)$$

and

$$\mu_s \equiv \frac{4\rho_s r_s}{\Sigma_{\text{cr}}}, \quad (64)$$

where  $\Sigma_{\text{cr}}$  is the critical surface mass density defined by equation (44). Note, here we use  $\xi_0 = r_s$  as the length unit in the lens plane,  $\eta_0 = r_s D_S^A / D_L^A$  as the length unit in the source plane. The dimensionless parameter  $\mu_s$  summarizes the ability for a GNFW halo to produce multiple images. Multiple images are formed if and only if  $|y| \leq y_{\text{cr}}$ , where  $y_{\text{cr}} \equiv -y(x_{\text{cr}})$ ,  $x_{\text{cr}} > 0$  is determined by  $dy/dx = 0$  (see Fig. 4). Let us consider the splitting angle  $\Delta\theta$  between the two outside images when more than two images are formed. For  $|y| < y_{\text{cr}}$ , there are three real roots of equation (62):  $x_1 > x_2 > x_3$ , then  $\Delta\theta \propto \Delta x \equiv x_1 - x_3$ . In general, the value of  $x_1 - x_3$  (and thus the value of  $\Delta\theta$ ) is insensitive to the value of  $y$  when  $|y| < y_{\text{cr}}$ <sup>1</sup>. So, we have

$$\Delta x(y) \approx \Delta x(y=0) = 2x_0, \quad \text{for } |y| < y_{\text{cr}}, \quad (65)$$

where  $x_0$  is the positive root of  $y(x) = 0$ . Then, for a GNFW lens at redshift  $z$ , the cross-section in the lens plane for forming multiple images with  $\Delta\theta > \Delta\theta_0$  is

$$\sigma(> \Delta\theta_0, M, z) \approx \pi y_{\text{cr}}^2 r_s^2 \vartheta(\Delta\theta - \Delta\theta_0). \quad (66)$$

The splitting angle  $\Delta\theta$  is given by

$$\Delta\theta = \frac{r_s}{D_L^A} \Delta x \approx \frac{2x_0 r_s}{D_L^A}. \quad (67)$$

For  $\alpha = 1$  (the NFW case) and  $\alpha = 2$  (the modified SIS case),  $g(x)$  defined by equation (63) can be worked out analytically. For  $\alpha = 1$ , we have

$$g(x) = \ln \frac{x}{2} + \begin{cases} \frac{1}{\sqrt{x^2-1}} \arctan \sqrt{x^2-1} & (x > 1), \\ \frac{1}{\sqrt{1-x^2}} \operatorname{arctanh} \sqrt{1-x^2} & (0 < x < 1), \\ 1 & (x = 1). \end{cases} \quad (68)$$

For  $\alpha = 2$ , we have

$$g(x) = \ln \frac{x}{2} + \frac{\pi}{2} x + \begin{cases} -\sqrt{x^2-1} \arctan \sqrt{x^2-1} & (x > 1), \\ \sqrt{1-x^2} \operatorname{arctanh} \sqrt{1-x^2} & (0 < x < 1), \\ 1 & (x = 1). \end{cases} \quad (69)$$

Equation (68) has also been obtained by Bartelmann (1996). For other values of  $\alpha$ ,  $g(x)$  has to be worked out numerically.

---

<sup>1</sup>See Schneider, Ehlers, & Falco (1992). For the extreme case of a singular isothermal sphere,  $\Delta x$  is exactly independent the position of the source object in the source plane when double images are formed, see equation [46].

## 4.2. Determination of $\rho_s$ and $r_s$

For a halo with a GFW profile, its mass diverges logarithmically as  $r \rightarrow \infty$ . So as usual, we define the mass of a halo to be the mass within  $r_{200}$

$$M = 4\pi \int_0^{r_{200}} \rho r^2 dr = 4\pi \rho_s r_s^3 f(c_1), \quad (70)$$

where  $c_1 \equiv r_{200}/r_s$  is the concentration parameter and

$$f(c_1) \equiv \int_0^{c_1} \frac{x^2 dx}{x^\alpha (1+x)^{3-\alpha}}. \quad (71)$$

For  $1 \leq \alpha \leq 2$ ,  $f(c_1)$  can be worked out analytically

$$f(c_1) \equiv \begin{cases} \ln(1+c_1) - \frac{c_1}{1+c_1} & (\alpha = 1), \\ \ln(1+c_1) & (\alpha = 2), \\ \frac{c_1^{3-\alpha}}{3-\alpha} {}_2F_1(3-\alpha, 3-\alpha; 4-\alpha; -c_1) & (1 < \alpha < 2), \end{cases} \quad (72)$$

where  ${}_2F_1$  is the hypergeometric function. From equation (35) and equation (70), we obtain

$$\rho_s = \rho_{\text{crit}} \frac{200}{3} \frac{c_1^3}{f(c_1)} = \rho_{\text{crit},0} [\Omega_m (1+z)^3 + \Omega_R (1+z)^2 + \Omega_\Lambda] \frac{200}{3} \frac{c_1^3}{f(c_1)}, \quad (73)$$

and

$$r_s = \frac{1}{c_1} \left( \frac{3M}{800\pi\rho_{\text{crit}}} \right)^{1/3} = \frac{1.626}{c_1} \frac{M_{15}^{1/3}}{[\Omega_m (1+z)^3 + \Omega_R (1+z)^2 + \Omega_\Lambda]^{1/3}} h^{-1} \text{Mpc}. \quad (74)$$

If we know the value of the concentration parameter  $c_1$ , with equation (73) and (74) we can determine  $\rho_s$  and  $r_s$  for any halo of mass  $M$  in any cosmology. Interestingly,  $\rho_s$  does not depend on the mass of the halo. To determine the value of  $c_1$  is not easy, and different methods give different results (Navarro, Frenk, & White 1997; Bartelmann et al. 1998). Various simulations suggest that  $c_1(z) \propto (1+z)^{-1}$  (Navarro & Steinmetz 2000; Bullock et al. 2001). Thus, here we assume that  $c_1(z) = c_1(z=0)/(1+z)$ , and we try to infer  $c_1(z=0)$  from simulation results. We take the values of  $c_1(z=0)$  for the NFW profile (i.e. the  $\alpha = 1$  case) from Bartelmann et al. (1998)'s simulation results, then obtain the values of  $c_1(z=0)$  for other cases (i.e.  $\alpha > 1$ ) by referencing the values for the NFW case. To do so, let us assume that fitting a dark halo with different density profiles gives the same ratio  $\eta \equiv r_{1/2}/r_{200}$ , where  $r_{1/2}$  is defined by  $M(r < r_{1/2}) = \frac{1}{2}M(r < r_{200})$ . Then we obtain a relation

$$\int_0^{\eta c_1(z=0)} \frac{x^2 dx}{x^\alpha (1+x)^{3-\alpha}} = \frac{1}{2} \int_0^{c_1(z=0)} \frac{x^2 dx}{x^\alpha (1+x)^{3-\alpha}}. \quad (75)$$

In equation (75),  $\eta$  is the same for all values of  $\alpha$ . So, with the known value of  $c_1$  for the  $\alpha = 1$  case – let us denote it with  $c_0$ , we can solve  $\eta = \eta(c_0)$  by equation (75). Then, since  $\eta$  is assumed to be the same for all the values of  $\alpha$ , we can solve  $c_1(z = 0) = c_1(\alpha, z = 0)$  by equation (75) for any  $1 < \alpha \leq 2$  with the  $\eta$  just solved. Then, we calculate  $c_1$  at any redshift with  $c_1(z) = c_1(z = 0)/(1 + z)$ .

According to Bartelmann et al. (1998), for the NFW profile, we choose

$$c_1(z = 0) = \begin{cases} 5, & \text{for SCDM} \\ 9, & \text{for OCDM} \\ 7, & \text{for LCDM} \end{cases} . \quad (76)$$

Then, according to the procedure described above, we obtain

$$c_1(z = 0) = \begin{cases} 2.7, & \text{for SCDM} \\ 5.3, & \text{for OCDM} \\ 4.0, & \text{for LCDM} \end{cases} \quad (77)$$

for a GFW profile with  $\alpha = 1.5$ , and

$$c_1(z = 0) = \begin{cases} 0.58, & \text{for SCDM} \\ 1.8, & \text{for OCDM} \\ 1.2, & \text{for LCDM} \end{cases} \quad (78)$$

for a GFW profile with  $\alpha = 2$ .

A critical parameter determining gravitational lensing is the surface mass density. A mass concentration with a central surface density larger than the surface density of the universe,  $\Sigma_{\text{cr}} \propto cH_0/G$  (see eq. [44]), can produce multiple images (Turner, Ostriker, & Gott 1984). While it is true that for  $\alpha \geq 1$  the surface density is divergent as  $r \rightarrow 0$  and thus, formally, all halos can produce multiple images, there may be very little mass contained within the  $\Sigma = \Sigma_{\text{cr}}$  contour. So, large splittings will not be common unless the surface density at the half-mass point is near  $\Sigma_{\text{cr}}$ . The mean surface density at the half-mass radius is

$$\begin{aligned} \Sigma_{1/2} &= \frac{M}{2\pi} \left( \frac{800\pi\rho_{\text{crit}}}{3M} \right)^{2/3} \frac{1}{\eta^2} \\ &= 0.0126 \frac{\text{g}}{\text{cm}^2} M_{15}^{1/3} h [\Omega_m(1+z)^3 + \Omega_R(1+z)^2 + \Omega_\Lambda] S(c_1), \end{aligned} \quad (79)$$

where  $S(c_1) \equiv \eta(c_1)^{-2}$ . For a fixed cosmology and a fixed mass  $\Sigma_{1/2}$  is proportional to  $S(c_1)$ . We plot this function in Fig. 5. The steep dependence of  $S(c_1)$  ( $\propto \Sigma/\Sigma_{\text{cr}}$ ) on  $c_1$  indicates that, for any assumed  $\alpha$ , more concentrated halos are much more effective in lensing.

Several authors have noted that the large concentrations indicated by high resolution N-body simulations of the CDM scenario (Navarro, Frenk, & White 1996, 1997; Moore et al. 1998) may be inconsistent with a variety of observations including the inner rotation curves of galaxies (Moore 1994; Flores & Primack 1994; De Block & McGaugh 1997; Tyson, Kochanski, & Dell’antonio 1998; Spergel & Steinhardt 2000). Here we note that if we alter, for whatever reasons, the concentration parameter from ten to five we will lower the characteristic half-mass surface density by a factor of  $\sim 1.5$  reducing greatly the fraction of mass in the universe contained in halos with a mean surface density exceeding the critical surface density, and thus reducing the probability of lensing by a large factor. This will be confirmed by the results in the next subsection. Recently, Bode, Ostriker, & Turok (2000) have performed detailed high-resolution N-body simulations of the warm dark matter (WDM) scenario to determine if this variant can successfully address the putative difficulties of the CDM paradigm. They find a significant decrease in concentration in the WDM scenario and also a decrease in the best fit value of  $\alpha$ .

### 4.3. Lensing probability by a generalized NFW model

Once  $\rho_s$  and  $r_s$  are determined, we can calculate  $\mu_s$  with

$$\mu_s = 2.0014 \times 10^{-3} \left( \frac{\rho_s}{\rho_{\text{crit},0}} \right) \left( \frac{r_s}{1h^{-1}\text{Mpc}} \right) \left( \frac{D_R^A}{c/H_0} \right), \quad (80)$$

where equations (44) and (64) have been used. With equations (62), (67), (73), (74), and (80), we can solve  $\Delta\theta = \Delta\theta(M, z)$  for any  $1 \leq \alpha \leq 2$ . In Fig. 6 we show  $\Delta\theta = \Delta\theta(M)$  produced by a NFW lens at  $z = 0.3$ , where the concentration parameters are given by equation (76). The source object is assumed to be at  $z_s = 1.5$ . For comparison, we also show the splitting angle produced by a SIS lens at the same redshift (thin lines in Fig. 6). The difference in the splitting angles produced by the two different mass density profiles is dramatic for small mass lenses: the splitting produced by a NFW lens is greatly shifted towards small angles. To produce the same small splitting angle a NFW halo requires more mass than a SIS halo. And, for the NFW case the difference in the results for different cosmological models are important – especially for low mass lenses, but for the SIS case the difference in the results for different cosmological models are unimportant.

The splitting angle  $\Delta\theta$  increases monotonically with increasing  $M$ , so  $\vartheta(\Delta\theta - \Delta\theta_0) = \vartheta(M - M_0)$ , where  $M_0$  is obtained by solving  $\Delta\theta(M_0, z) = \Delta\theta_0$ . Then, from equation (54) and equation (66), the differential lensing probability by a GNFW profile is

$$\frac{d}{dz}P(> \Delta\theta_0) = 2.614 \Omega_m (1+z)^3 \frac{d}{dz} \left( \frac{D_L}{c/H_0} \right)$$

$$\times \int_{M_0}^{\infty} f(M_{15}, z) y_{\text{cr}}^2 \left( \frac{r_s}{1h^{-1}\text{Mpc}} \right)^2 \frac{dM_{15}}{M_{15}}. \quad (81)$$

The integral lensing probability is calculated with equation (52) and equation (81).

We have calculated the lensing probabilities for different cosmologies and different GNFW halos. Our results are summarized in Fig. 7 – Fig. 10, where the source object is assumed to be at  $z_s = 1.5$ , the Hubble constant is taken to be  $h = 0.7$ ,  $\sigma_8$  and  $\Omega_m$  are constrained by equation (22).

Fig. 7 shows the differential lensing probability  $dP/dz$  for  $\Delta\theta > 5''$  as a function of lenses' redshift  $z$ . The three cosmological models are: SCDM with  $\Omega_m = 1$  and  $\sigma_8 = 0.5$ ; OCDM with  $\Omega_m = 0.3$ ,  $\Omega_\Lambda = 0$ , and  $\sigma_8 = 0.85$ ; LCDM with  $\Omega_m = 0.3$ ,  $\Omega_\Lambda = 0.7$ , and  $\sigma_8 = 0.95$ . Three cases with different values of  $\alpha$  are shown:  $\alpha = 1$  (i.e. the NFW case), 1.5, and 2. The concentration parameters of halos are determined with the procedure described in the last subsection, i.e. they are given by equation (76), equation (77), and equation (78). Similar to the case for SIS halos (see Fig. 2) and independent of the parameter  $\alpha$  of GNFW halos, the differential lensing probability peaks at intermediate redshifts: at  $z \approx 0.3$  for SCDM, at  $z \approx 0.4$  for OCDM and LCDM. Fig. 8 shows the integral lensing probability  $P(> \Delta\theta)$  as a function of the splitting angle  $\Delta\theta$ , for the same models in Fig. 7. As  $\alpha$  decreases (i.e. as the halo central density becomes more shallow), Fig. 8 shows, the lensing probability drops quickly. NFW halos are least efficient in producing multiple images among halos with  $1 \leq \alpha \leq 2$ . Furthermore, as  $\alpha$  decreases, the difference between the SCDM cosmological model and the OCDM/LCDM model becomes more prominent: for the NFW case the lensing probability for the SCDM model is lower than the lensing probability for the OCDM/LCDM model by two orders of magnitude, though the difference between the OCDM model and the LCDM model is not so big. This is due to the fact that the lensing probability for the NFW case is extremely sensitive to the concentration parameter of halos and the mass fluctuation  $\sigma_8$ , a halo in a SCDM universe has the smallest concentration parameter  $c_1$  (see eq. [76]), and the SCDM model has the smallest  $\sigma_8$ . Fig. 8 shows one of our most important results. If  $\alpha$  is the same for all halos, then one expects that, in the OCDM/LCDM case, the number of  $10''$  splittings observed to be only slightly less than the number of  $1''$  splittings observed.

The sensitivity of the lensing probability to the concentration parameter is shown in Fig. 9, where the models are the same in Fig. 7 and Fig. 8 except that in Fig. 9 we allow the concentration parameter to vary from 2 to 15. Fig. 9 shows that the sensitivity of the lensing probability to the concentration parameter increases quickly as  $\alpha$  and  $c_1$  decrease. Fig. 10 shows the dependence of the lensing probability  $P(> 5'')$  on the cosmic mass density  $\Omega_m$  when  $\Omega_m$  and  $\sigma_8$  are correlated through equation (22), the observed cluster number

constraints. Though the correlation in equation (22) is confirmed by the statistics of cluster abundances, we see some breakup of this relation in lensing statistics. The breakup is most prominent for the NFW case.

## 5. Comparison with Observations

To compare with observations we must consider the effect of magnification bias (Turner, Ostriker, & Gott 1984; Kochanek 1995; Bartelmann & Schneider 2001). According to Turner, Ostriker, & Gott (1984), the factor  $B$  by which lensed objects at redshift  $z_s$  will be overrepresented in any particular observed sample may be written as

$$B = \frac{\int_0^\infty S(f) \int_{A_m}^\infty A^{-1} P(A) N_{z_s}(f/A) dA df}{\int_0^\infty S(f) N_{z_s}(f) df}, \quad (82)$$

where  $f$  is the observable flux of source objects,  $S(f)$  is the selection function,  $A_m$  is the minimum total flux amplification for a multiple imaged source object,  $P(A)$  is the probability density for a greater amplification  $A$ , and  $N_{z_s}(f)df$  is the number of source objects in the sky at redshift  $z_s$  with unlensed flux lying between  $f$  and  $f + df$ . If the sample of source objects has a flux distribution with a single power-law  $N_{z_s} \propto f^{-\beta}$ , the calculation of the magnification bias factor becomes extremely simple

$$B = \int_{A_m}^\infty A^{\beta-1} P(A) dA, \quad (83)$$

which is independent of the selection function. Quite generally  $P(A)$  is given by  $P(A) = 2A_m^2 A^{-3}$  for  $A \geq A_m$  (Turner, Ostriker, & Gott 1984; Schneider, Ehlers, & Falco 1992). Then, if the sample of source objects has a power-law flux distribution, the magnification bias is simply

$$B = \frac{2}{3 - \beta} A_m^{\beta-1}. \quad (84)$$

For a SIS lens the total magnification is  $A = 2/|y|$  so  $A_m = 2$  since multiple images are formed only if  $y \leq 1$  (Turner, Ostriker, & Gott 1984; Schneider, Ehlers, & Falco 1992). For a NFW or GNFW lens, the calculation of the total magnification is straightforward but complex, and to determine its minimum is not easy. Here we estimate the minimum of the total magnification for a NFW/GNFW lens with

$$A_m \approx \frac{2x_0}{y_{\text{cr}}}, \quad (85)$$

where  $x_0$  is the positive root of  $y(x) = 0$ ,  $y_{\text{cr}} = -y(x_{\text{cr}})$  and  $x_{\text{cr}}$  is the positive root of  $dy/dx = 0$  (see subsection 4.1 and Fig. 4). Note equation (85) is accurate for a SIS lens. Using equation (66) and equation (67), equation (85) can be written as

$$A_m \approx \Delta\theta D_L^A \left(\frac{\pi}{\sigma}\right)^{1/2}, \quad (86)$$

where  $\sigma$  is the lensing cross-section.

For a SIS lens  $A_m = 2$  which is a constant number, thus  $B$  is independent of the redshift and mass of the lens and the observable lensing probability  $P_{\text{obs}}$  is related to the intrinsic lensing probability  $P$  simply by  $P_{\text{obs}} = BP$  (Turner, Ostriker, & Gott 1984). But for a NFW/GNFW lens,  $A_m$  and  $B$  depend on both the redshift and the mass of the lens, thus  $P_{\text{obs}}$  is related to  $P$  by an integration

$$P_{\text{obs}}(> \Delta\theta) = \int \int B \frac{d^2 P(> \Delta\theta)}{dM dz}, \quad (87)$$

where the intrinsic lensing probability  $P$  is given by equation (52) and equation (53). The average magnification bias  $\bar{B} \equiv P_{\text{obs}}/P$  is then a function of  $\Delta\theta$ .

Currently the largest uniformly selected sample of gravitational lensing system is the Cosmic Lens All-Sky Survey (CLASS; Browne & Myers 2000). The sample comprises 11685 flat-spectrum radio sources whose flux distribution is given by a power-law  $N_{z_s}(f) \propto f^{-2.1}$  (Helbig 2000; Rusin & Tegmark 2000). The redshift distribution of the CLASS sample is not known, but Marlow et al. (2000) has reported redshifts for a small subsample of 42 sources. They have found a mean source redshift of  $\langle z_s \rangle = 1.27$ , which is comparable to that found in other radio surveys at comparable fluxes. To date a total of 18 multiple image gravitational lenses have been discovered in the combined JVAS<sup>2</sup> and CLASS sample, all have image separations  $\Delta\theta < 3''$  (Browne & Meyer 2000; Helbig 2000). An explicit search for lenses with images separations  $6'' \leq \Delta\theta \leq 15''$  has found no lenses (Phillips et al. 2000). Among the 18 discovered lens systems, one (B2114+022) is questionable (Helbig 2000) so we exclude it from our analyses. The remaining 17 lens systems are shown in Fig. 11 as a histogram.

To compare our results with the CLASS survey, we assume all source objects in the sample are at  $z_s = 1.27$ . For the CLASS sample  $\beta \approx 2.1$  (Rusin & Tegmark 2000), so from equation (84) we have

$$B \approx 2.22 A_m^{1.1}. \quad (88)$$

---

<sup>2</sup>Jodrell-VLA Astrometric Survey, see King et al. (1999) and references therein.



For SIS lenses  $A_m = 2$ , then we have  $B \approx 4.76$ . For NFW/GNFW lenses we calculate  $A_m$  and  $B$  using equation (86) and equation (88). Then we calculate the observable lensing probability using equation (87). The results for SIS lenses and NFW lenses are shown in Fig. 11 alternatively for SCDM with  $\Omega_m = 1$  and  $\sigma_8 = 0.5$ ; OCDM with  $\Omega_m = 0.3$ ,  $\Omega_\Lambda = 0$ , and  $\sigma_8 = 0.85$ ; LCDM with  $\Omega_m = 0.3$ ,  $\Omega_\Lambda = 0.7$ , and  $\sigma_8 = 0.95$ . Again, we assume the Hubble constant  $h = 0.7$ . The concentration parameters for the NFW lenses are  $c_1 = 5$  for SCDM, 9 for OCDM, and 7 for LCDM. For comparison, we have also shown the result for a LWDM model with a dashed-dotted curve, which has the same parameters as the LCDM model except that for the LWDM we assume a power-law spectrum  $P_k \propto k^{-2}$  and take a smaller concentration parameter  $c_1 = 3.5$ . The null results for the JVAS/CLASS survey for  $6'' \leq \Delta\theta \leq 15''$  is shown with a horizontal straight line with a downward arrow indicating that is an upper limit. Fig. 11 clearly shows that, all SIS models predict too many lenses for large splitting angles. While for large splitting angles NFW models are consistent with the JVAS/CLASS results in the sense that the NFW predictions are below the upper limit put by JVAS/CLASS, for small splitting angles the NFW predictions are far below the observational results of JVAS/CLASS. So, both SIS models and NFW models cannot explain the observations. We have also tried GNFW models with  $1 < \alpha < 2$ , neither of them can explain the observations on both small splitting angles and large splitting angles. All the models either predict too many lenses with large splitting angles, or too few lenses with small splitting angles. Neither of them can produce the observed large ratio of the number of small splittings to the number of large splittings.

For the same cosmological and lens models we have also calculated the average magnification bias  $\overline{B} = P_{\text{obs}}/P$ , the results for NFW models and SIS models are shown in Fig. 12. We see that, the magnification bias for NFW lenses is bigger than the magnification bias for SIS lenses by about one order of magnitude. Though the magnification bias for SIS lenses is a constant for all cosmological models, the magnification bias for NFW lenses depends on cosmological models and slowly decreases as the splitting angle increases.

The above results strongly suggest that the halos in the real universe cannot be described by a single universal density profile. There must be at least two populations of “halos” in the universe: small mass halos with a steep inner density slope, and large mass halos with a shallow inner density slope. To test this conjecture, we have calculated the following additional lens model: lenses with mass  $M < M_c$  have the SIS profile (which would produce the flat rotation curves seen in galaxies), but lenses with mass  $M > M_c$  have the NFW profile. The critical mass  $M_c$  for transition from SIS to NFW is determined by fitting our results with the JVAS/CLASS observations. Our fitting results indicate that  $M_c \sim 10^{13} h^{-1} M_\odot$ . Interestingly, this critical mass is very close to the cutoff mass of halos below which cooling of the corresponding baryonic component will lead to concentration of the baryons to the inner

parts of the mass profile (Rees & Ostriker 1977; Blumenthal et al. 1986; Porciani & Madau 2000). The results for the case with  $M_c = 10^{13} h^{-1} M_\odot$  are shown in Fig. 13, which fit the JVAS/CLASS observations reasonably well. The cosmological models are the same as those in Fig. 11. The NFW halos (with  $M > 10^{13} h^{-1} M_\odot$ ) have the same concentration parameters as those in Fig. 11. Though all the three models are consistent with the JVAS/CLASS  $6'' - 15''$  survey, the SCDM model obviously produces too many lenses with small splitting angles. It is interesting that while SCDM produces the most small splittings, it produces the fewest large splittings. We have calculated the expected total number of lenses with  $\Delta\theta > 0.3''$  for the JVAS/CLASS sample, the results are

$$N_{\text{lens}}(> 0.3'') = \begin{cases} 37, & \text{for SCDM} \\ 12, & \text{for OCDM} \\ 16, & \text{for LCDM} \end{cases} . \quad (89)$$

The expected number of lenses for the LCDM model is remarkably close to the number of lenses observed by the JVAS/CLASS survey which is 17 if we exclude the questionable lens of B2114+022 from the sample.

## 6. Discussion and Conclusions

With the semi-analytical approach we have calculated the probability for forming multiple images of a remote source object gravitationally lensed by foreground dark halos. The mass density profile of a halo is alternatively taken to be described by the SIS profile, the NFW profile, and the GNFW profile. The mass function of halos is assumed to be given by the Press-Schechter function. The cosmological model is alternatively the SCDM model, the OCDM model, and the LCDM model. Our results show that the lensing probability is very sensitive to the density profile of lenses (dark halos). The more the mass distribution concentrates toward the center, the higher lensing probability the density profile gives rise, which is clearly seen in Fig. 7 – Fig. 10. Compared to SIS lenses, NFW lenses are extremely inefficient in producing multiple images. For example, the lensing probability  $P(> 5'')$  for NFW halos is lower than the corresponding probability for SIS halos by more than two orders of magnitudes. For GNFW halos, as  $\alpha$  decreases, the differences among different cosmological models become prominent (Fig. 8), especially the difference between the SCDM model and the OCDM/LCDM model: when  $\alpha = 1$  (i.e. for NFW halos) the lensing probability for the SCDM model is lower than the lensing probability for the OCDM/LCDM model by more than two orders of magnitudes. This dramatic effect is dominantly caused by the fact that halos in a SCDM universe have the smallest concentration parameter (Bartelmann et al. 1998) and for smaller  $\alpha$  the lensing probability is more sensitive to the concentration

parameter  $c_1$ : for the NFW case the lensing probability is extremely sensitive to  $c_1$ , especially for small  $c_1$  (Fig. 9). Though not so dramatic as the dependence on the inner slope, the lensing probability also shows dependence on the outer slope of halos. Comparing the right panel of Fig. 8 with Fig. 3, the lensing probability produced by GFW halos with  $\alpha = 2$  is somewhat higher than the lensing probability produced by SIS halos. This mild difference is attributed to the different slopes of the  $\alpha = 2$ , GFW profile and the SIS profile at large radii (the  $\alpha = 2$ , GFW profile and the SIS profile have the same slope at small radii). Similar conclusions are obtained by Wyithe, Turner, & Spergel (2000) and Keeton & Madau (2001). Wyithe, Turner, & Spergel (2000) find that the optical depth to multiple imaging is a very sensitive function of the profile parameters and the GFW profile exhibits degeneracies between profile parameters with respect to lensing statistics. Keeton & Madau (2001) demonstrate that the lensing probability is determined almost entirely by the fraction of the halo mass that is contained within a fiducial radius that is  $\sim 4\%$  of the virial radius.

Our results also show the dependence of the lensing probability on the cosmological parameters, which is particularly manifested in the SIS case. In Fig. 3, for small splitting angles the lensing probability in the SCDM universe is higher than the lensing probability in the  $\Lambda$ CDM/LCDM universe, while for large splitting angles the lensing probability in the SCDM universe is much lower than the lensing probability in the  $\Lambda$ CDM/LCDM universe. This is explained by the fact that the Press-Schechter function is sensitive to  $\sigma_8$  only for large mass halos (Fig. 1). Since small splitting angles are produced by small mass halos, and for small mass halos the Press-Schechter function is not sensitive to  $\sigma_8$ , the lensing probability is dominantly determined by the cosmic mean mass density  $\Omega_m$ ; thus for small splitting angles the lensing probability is highest for SCDM since the SCDM universe has the highest mean mass density. Since large splitting angles are produced by large mass halos and for large mass halos the Press-Schechter function is (exponentially) sensitive to  $\sigma_8$ , the lensing probability is dominantly determined by  $\sigma_8$ , thus for large splitting angles the lensing probability is lowest for SCDM since the SCDM universe has the smallest  $\sigma_8$ . For the NFW case, in Fig. 6 we see that to produce the same small splitting angle the required NFW halo mass is significantly larger than the required SIS halo mass. Thus, for the NFW case  $\sigma_8$  takes effect for all  $\Delta\theta \geq 1''$ , which together with the concentration parameter  $c_1$  overtakes the effect of  $\Omega_m$  (see Fig. 8). The studies of cluster abundances proposed a correlation between  $\Omega_m$  and  $\sigma_8$  as given by equation (22). We have also tested the sensitivity of the lensing probability to  $\Omega_m$  when equation (22) is satisfied. We see that in general the lensing probability varies with  $\Omega_m$ ; and for the NFW case the lensing probability is very sensitive to  $\Omega_m$  (Fig. 10).

Our numerical results are summarized in Table 1, where we have not included the effect of magnification bias (i.e.  $P$  is the intrinsic probability), the source object is assumed to be

at  $z_s = 1.5$ , the Hubble constant is assumed to be  $h = 0.7$ . To show the sensitivity of the lensing probability to the parameters  $\sigma_8$ ,  $\Omega_m$ ,  $\alpha$ , and  $c_1$ , we have evaluated the differentiation of lensing probability  $P(> \Delta\theta)$  with respect to  $\sigma_8$ ,  $\Omega_m$ ,  $\alpha$ , and  $c_1$  for the LCDM model at  $\sigma_8 = 0.95$ ,  $\Omega_m = 0.3$ ,  $\Omega_\Lambda = 0.7$ ,  $\alpha = 1.5$ , and  $c_1(z = 0) = 4$  for  $\Delta\theta = 5''$  and  $\Delta\theta = 10''$  respectively. The results are

$$\begin{aligned} \frac{\delta P}{P} = & 4.9 \left( \frac{\delta\sigma_8}{\sigma_8} \right)_{\Omega_m, \alpha, c_1} + 1.7 \left( \frac{\delta\Omega_m}{\Omega_m} \right)_{\sigma_8, \alpha, c_1} + 11 \left( \frac{\delta\alpha}{\alpha} \right)_{\sigma_8, \Omega_m, c_1} \\ & + 3.1 \left( \frac{\delta c_1}{c_1} \right)_{\sigma_8, \Omega_m, \alpha}, \end{aligned} \quad (90)$$

for  $\Delta\theta = 5''$ , and

$$\begin{aligned} \frac{\delta P}{P} = & 5.8 \left( \frac{\delta\sigma_8}{\sigma_8} \right)_{\Omega_m, \alpha, c_1} + 1.8 \left( \frac{\delta\Omega_m}{\Omega_m} \right)_{\sigma_8, \alpha, c_1} + 10 \left( \frac{\delta\alpha}{\alpha} \right)_{\sigma_8, \Omega_m, c_1} \\ & + 3.4 \left( \frac{\delta c_1}{c_1} \right)_{\sigma_8, \Omega_m, \alpha}, \end{aligned} \quad (91)$$

for  $\Delta\theta = 10''$ . Note the extreme sensitivity of the lensing probability to the slope of the inner profile:  $(d \ln P / d \ln \alpha)_{\sigma_8, \Omega_m, c_1} \approx 10$ . Note also that, if  $\Omega_m$  and  $\sigma_8$  enter the lensing probability as a combination given by equation (22), then we should expect  $(d \ln \sigma_8 / d \ln \Omega_m)_{P, \alpha, c_1} \approx \gamma \approx 0.53$ , but equation (90) and equation (91) show rather smaller values of  $(d \ln \sigma_8 / d \ln \Omega_m)_{P, \alpha, c_1}$  (0.34 and 0.31 respectively). Thus, in lensing statistics the degeneracy between  $\Omega_m$  and  $\sigma_8$  in equation (22) is broken. This is important since it allows us to separately determine the values of  $\Omega_m$  and  $\sigma_8$  in principle.

With the magnification bias being considered, none of the simple models can completely explain the JVAS/CLASS observations. The SIS models produce too many large splitting lenses, but the JVAS/CLASS observations have detected no lenses with  $\Delta\theta > 3''$  (Helbig 2000; Phillips et al. 2000). The null result for detecting large splitting lenses are true not only for JVAS/CLASS (Phillips et al. 2000), but also for ARCS (Arcminute Radio Cluster-lens Search) which is aimed at looking for gravitational lensing events with images separation between  $15''$  and  $60''$  (Phillips, Browne, & Wilkinson 2000). While the NFW models produce very rare large splitting lenses which is consistent with observations, they produce too few small splitting lenses which is against observations since in the JVAS/CLASS survey at least 17 lenses with  $0.3'' < \Delta\theta < 3''$  have been discovered (Helbig 2000). None of the models can explain the observable large ratio of the number of small splittings to the number of large splittings. This strongly suggests that there are at least two populations of halos in the universe: small mass halos with a steep inner density slope, and large mass halos with a shallow inner slope. We have constructed a very simple two-population halo model

to test this conjecture: the mass density of halos with mass  $< 10^{13} h^{-1} M_{\odot}$  is given by the SIS profile, while the mass density of halos with mass  $> 10^{13} h^{-1} M_{\odot}$  is given by the NFW profile. We find that the results for this model are reasonably consistent with the JVAS/CLASS observations. In particular, the number of lenses with  $\Delta\theta > 0.3''$  predicted by the LCDM model is  $\approx 16$ , which is remarkably close to the number of lenses observed by the JVAS/CLASS survey which is 17. The SIS model predicts too many lenses ( $\approx 37$ ), while the OCDM model predicts somewhat too few lenses ( $\approx 12$ ). A similar compound model has also been considered by Porciani & Madau (2000) to explain the results from CASTLE (CfA-Arizona Space Telescope Lens) survey.

In summary, with the semi-analytical approach we have shown that the gravitational lensing probability is very sensitive to the mass density profile of lenses (especially in the central region), the mean mass density in the universe, and the amplitude of primordial fluctuations. Compared with the observation results of JVAS/CLASS, our calculations indicate that the halos in the real universe cannot be described by a single universal density profile, there are at least two populations of halos in the universe: small mass halos with a steep inner density slope and large mass halos with a shallow inner density slope. Ultimately, of course, very accurate address of the question is left open by this study.

We are grateful to E. L. Turner for many helpful discussions and comments, to C. R. Keeton and P. Madau for helpful communications. We would like to thank the anonymous referee whose comments led to the improvement of this work. This research was supported by the NSF grants ASC-9740300 (subaward 766) and AST-9803137.

## REFERENCES

- Bahcall, N. A., & Cen, R. Y. 1993, *ApJ*, 407, L49
- Bartelmann, M. 1996, *A&A*, 313, 697
- Bartelmann, M., & Schneider, P. 2001, *Phys. Rep.*, 340, 291
- Bartelmann, M., & Weiss, A. 1994, *A&A*, 287, 1
- Bartelmann, M., Huss, A., Colberg, J. M., Jenkins, A., & Pearce, F. R. 1998, *A&A*, 330, 1
- Blumenthal, G. R., Faber, S. M., Flores, R., & Primack, J. R. 1986, *ApJ*, 301, 27
- Bode, P., Ostriker, J. P., & Turok, N. 2000, *astro-ph/0010389*

- Browne, I. W. A., & Meyers, S. T. 2000, in *New Cosmological Data and the Values of the Fundamental Parameters*, IAU Symposium, 201, 47
- Bullock, J. S., Kolatt, T. S., Sigad, Y., Somerville, R. S., Kravtsov, A. V., Klypin, A. A., Primack, J. R., Dekel, A. 2001, *MNRAS*, 321, 559
- Cen, R., Gott, J. R., Ostriker, J. P., & Turner, E. L. 1994, *ApJ*, 423, 1
- Chiu, W. A., Ostriker, J. P., & Strauss, M. 1998, *ApJ*, 494, 479
- Cooray, A. R. 1999, *ApJ*, 524, 504
- Crone, M., Evrard, A. E., & Richstone, D. O. 1994, *ApJ*, 434, 402
- De Block, W. J. G., & McGaugh, S. S. 1997, *MNRAS*, 290, 533
- Eisenstein, D. J., & Hu, W. 1999, *ApJ*, 511, 5
- Efstathiou, G. 1990, in *Physics of the Early Universe*, ed. J. A. Peacock, A. F. Heavens, & A. T. Davies (Edinburgh: SUSSP Publications), 361
- Efstathiou, G. P., Frenk, C. S., White, S. D. M., & Davis, M. 1988, *MNRAS*, 235, 715
- Eke, V. R., Cole, S., & Frenk, C. S. 1996, *MNRAS*, 282, 263
- Flores R. A., & Primack, J. A. 1994, *ApJ*, 427, L1
- Frenk, C. S., White, S. D. M., Davis, M., & Efstathiou, G. P. 1988, *ApJ*, 327, 507
- Frenk, C. S., White, S. D. M., Efstathiou, G. P., & Davis, M. 1985, *Nature*, 317, 595
- Ghigna, S., Moore, B., Governato, F., Lake, G., Quinn, T., & Stadel J. 1999, *ApJ*, 544, 616
- Girardi, M., Borgani, S., Giuricin, G., Mardirossian, F., & Mezzetti, M. 1998, *ApJ*, 506, 45
- Girardi, M., & Giuricin, G. 2000, *ApJ*, 540, 45
- Gott, J. R., & Gunn, J. E. 1974, *ApJ*, 190, L105
- Helbig, P. (for the CLASS collaboration) 2000, astro-ph/0008197
- Jing, Y. P., & Suto, Y. 2000, *ApJ*, 529, L69
- Kaufmann, R., & Straumann, N. 2000, *Annals Phys.*, 11, 507
- Kauffmann, G., & White, S. D. M. 1993, *MNRAS*, 261, 921

- Keeton, C. R., & Madau, P. 2001, astro-ph/0101058
- King, L. J., Browne, I. W. A., Marlow, D. R., Patnaik, A. R., & Wilkinson, P. N. 1999, MNRAS, 307, 225
- Klypin, A. 2000, astro-ph/0005504
- Kochanek, C. S. 1995, ApJ, 453, 545
- Kolb, E. W., & Turner, M. S. 1990, The Early Universe (Redwood City: Addison-Wesley Publishing Company)
- Lacey, C., & Cole, S. 1993, MNRAS, 262, 627
- Longair, M. S. 1998, Galaxy Formation (Berlin: Springer-Verlag)
- Maoz, D., Rix, H. -W., Gal-Yam, A., & Gould, A. 1997, ApJ, 486, 75
- Marlow, D. R., Rusin, D., Jackson, N., Wilkinson, P. N., & Browne, I. W. A. 2000, AJ, 119, 2629
- Meneghetti, M., Bolzonella, M., Bartelmann, M., Moscardini, L., & Tormen, G. 2000, astro-ph/0008483
- Moore, B. 1994, Nature (London), 370, 629
- Moore, B., Governato, F., Quinn, T., Stadel, J., & Lake, G. 1998, ApJ, 499, L5
- Mortlock, D. J., & Webster, R. L. 2000, astro-ph/0008081
- Narayan, R., & White, S. D. M. 1988, MNRAS, 231, 97p
- Navarro, J. F., & Steinmetz, M. 2000, ApJ, 528, 607
- Navarro, J. F., Frenk, C. S., & White, S. D. M. 1996, ApJ, 462, 563
- Navarro, J. F., Frenk, C. S., & White, S. D. M. 1997, ApJ, 490, 493
- Ostriker, J. P., & Steinhardt, P. J. 1995, Nature, 377, 600
- Peebles, P. J. E. 1980, The Large-Scale Structure of the Universe (Princeton: Princeton University Press)
- Peebles, P. J. E. 1993, Principles of Physical Cosmology (Princeton: Princeton University Press)

- Phillips, P. M., Browne, I. W. A., & Wilkinson, P. N. 2000, astro-ph/0009366
- Phillips, P. M., Browne, I. W. A., Wilkinson, P. N., & Jackson, N. J. 2000, astro-ph/0011032
- Porciani, C., & Madau, P. 2000, ApJ, 532, 679
- Press, W. H., & Schechter, P. 1974, ApJ, 187, 425
- Quinn, P. J., Salmon, J. K., & Zurek, W. H. 1986, Nature, 322, 329
- , Rees, M. J., & Ostriker, J. P. 1977, MNRAS, 179, 541
- Rusin, D., & Tegmark, M. 2000, astro-ph/0008329
- Schneider, P., Ehlers, J., & Falco, E. E. 1992, Gravitational Lenses (Berlin: Springer-Verlag)
- Spergel, D. N., & Steinhardt, P. J. 2000, Phys. Rev. Lett, 84, 3760
- Subramanian, K., Cen, R., & Ostriker, J. P. 2000, ApJ, 538, 528
- Turner, E. L. 1990, ApJ, 365, L43
- Turner, E. L., Ostriker, J. P., & Gott, J. R. 1984, ApJ, 284, 1
- Tyson, J. A., Kochanski, G. P., & Dell’antonio 1998, ApJ, 498, L107
- Wambsganss, J., Cen, R., Ostriker, J. P., & Turner, E. L. 1995, Sciences, 268, 274
- Wambsganss, J., Cen, R., & Ostriker, J. P. 1998, ApJ, 494, 29
- Wang, L., & Steinhardt, P. J. 1998, ApJ, 508, 483
- Wang, L., Caldwell, R. R., Ostriker, J. P., & Steinhardt, P. J. 2000, ApJ, 530, 17
- Warren, M. S., Quinn, P. J., Salmon, J. K., & Zurek, W. H. 1992, ApJ, 399, 405
- Wyithe, J. S. B., Turner, E. L., & Spergel, D. N. 2000, astro-ph/0007354
- Zhao, H. S. 1996, MNRAS, 278, 488
- Zurek, W. H., Quinn, P. J., & Salmon, J. K. 1988, ApJ, 330, 519



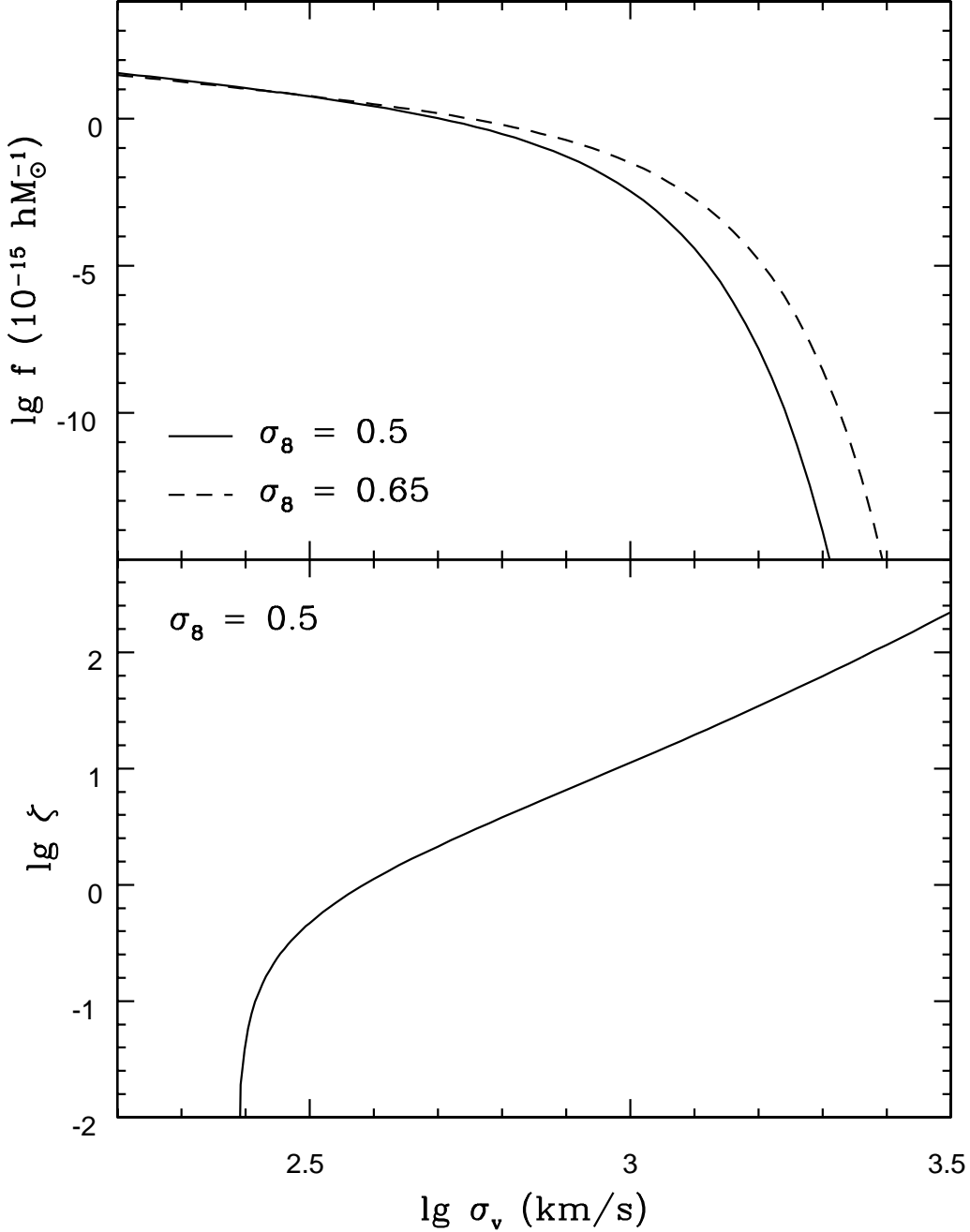


Fig. 1.— Upper panel: The Press-Schechter function  $f$  against the velocity dispersion  $\sigma_v$  of dark halos at  $z = 0$  in a SCDM cosmology. The solid curve is for  $\sigma_8 = 0.5$ , the dashed curve is for  $\sigma_8 = 0.6$ . Lower panel:  $\zeta \equiv \frac{\delta f/f}{\delta \sigma_8/\sigma_8}$  as a function of  $\sigma_v$ , for a SCDM cosmology with  $z = 0$  and  $\sigma_8 = 0.5$ . Both panels show that for large  $\sigma_v$ , a poor knowledge in  $f$  may give a good estimation of  $\sigma_8$ . Since lensing is produced by the high  $\sigma_v$  part of the distribution, the number of lenses sensitively constrains  $\sigma_8$ .

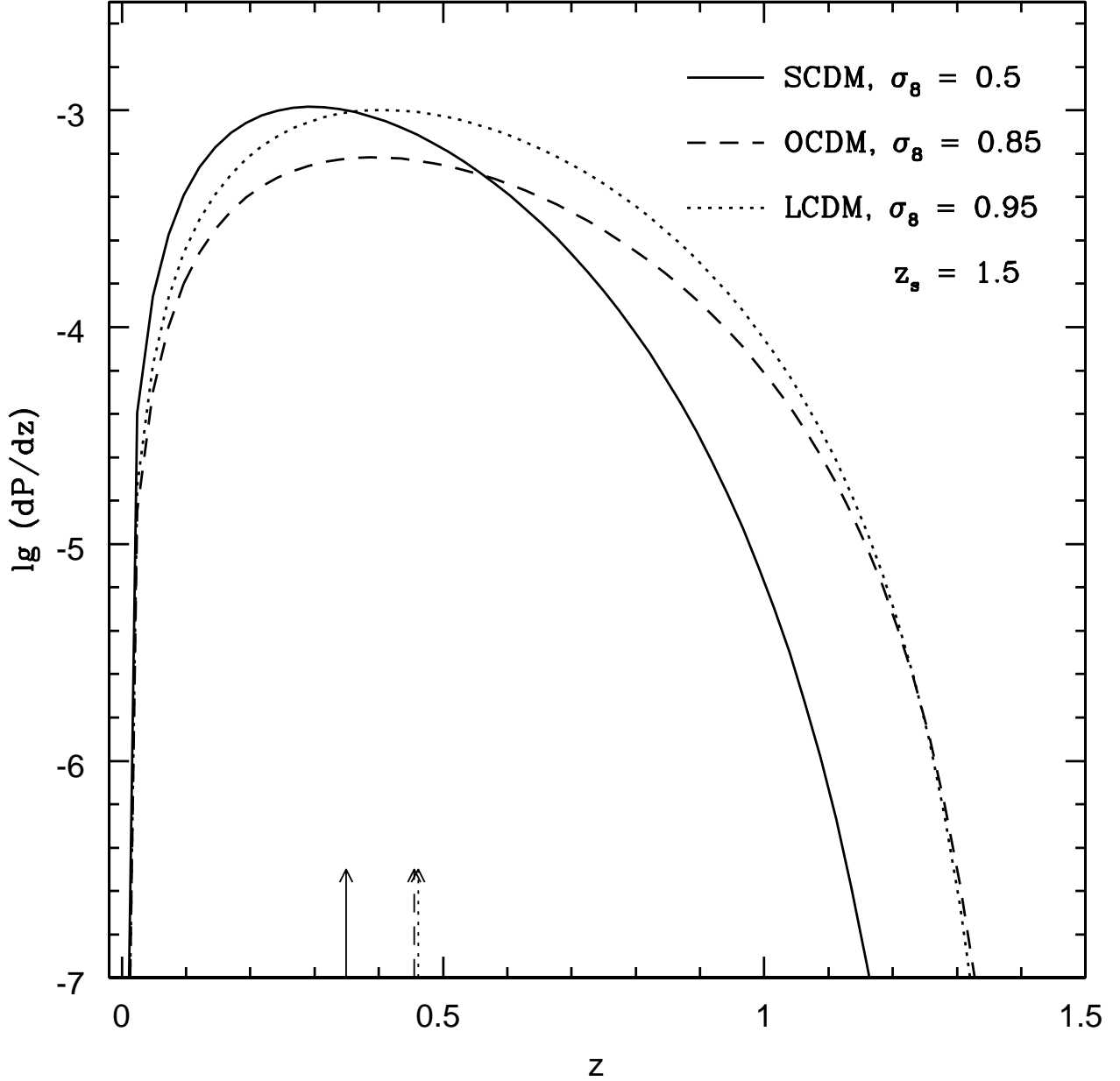


Fig. 2.— The differential lensing probability  $dP/dz$  for  $\Delta\theta > 5''$  as a function of lenses' redshift  $z$ . The source object is assumed to be at  $z_s = 1.5$ . The lens objects are SIS halos. The cosmological models are alternatively: SCDM with  $\Omega_m = 1$  and  $\sigma_8 = 0.5$  (solid line); OCDM with  $\Omega_m = 0.3$ ,  $\Omega_\lambda = 0$ , and  $\sigma_8 = 0.85$  (dashed line); LCDM with  $\Omega_m = 0.3$ ,  $\Omega_\lambda = 0.7$ , and  $\sigma_8 = 0.95$  (dotted line). The Hubble constant is  $h = 0.7$ . As expected, the probable position of the lens is at significantly higher redshifts for the low  $\Omega_m$  models than for SCDM – note arrows which show median expected redshifts.

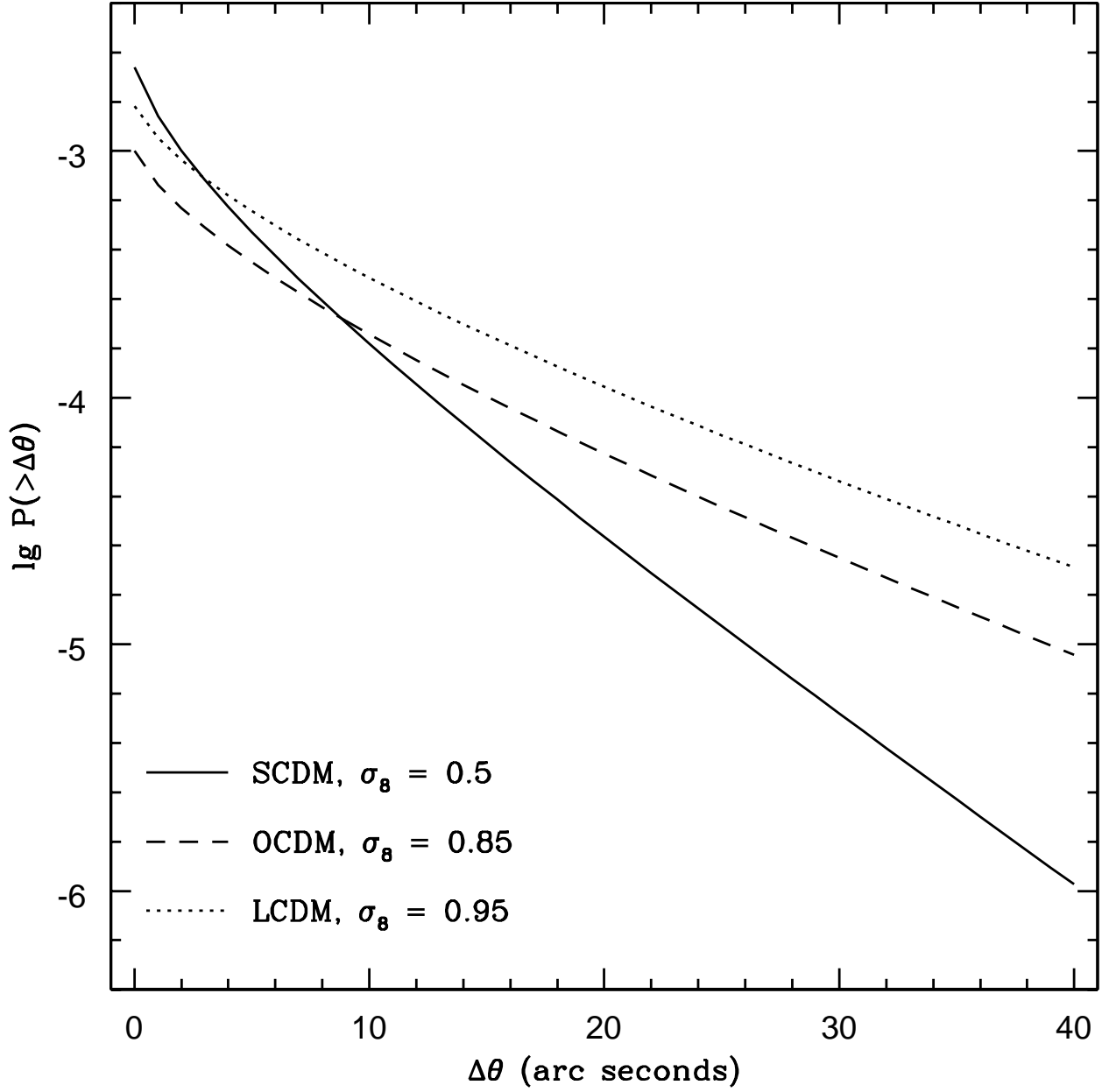


Fig. 3.— The integral lensing probability  $P(> \Delta\theta)$  as a function of  $\Delta\theta$ . The models are the same as those in Fig. 2.

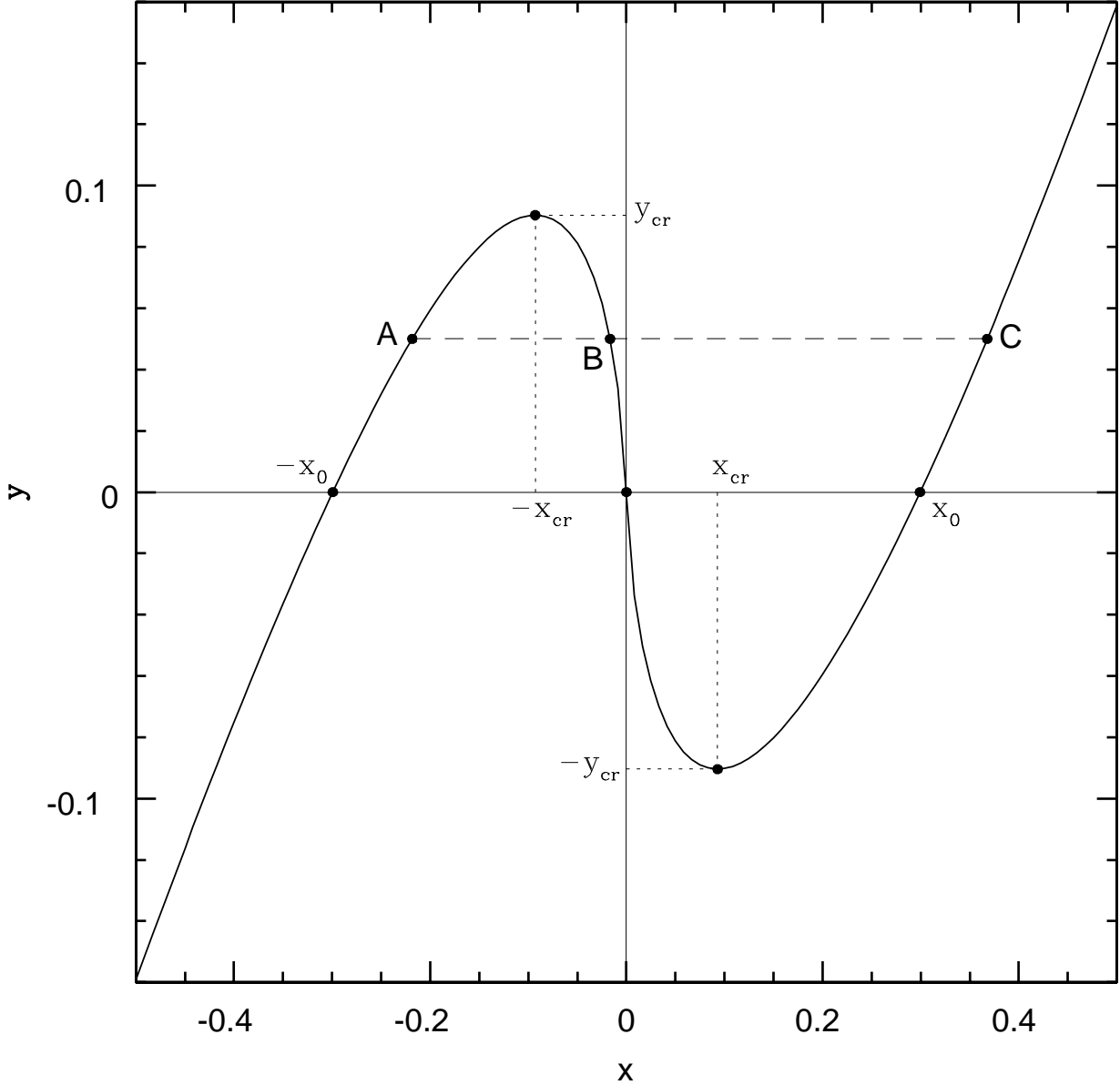


Fig. 4.— The lensing equation for the GFW profile, i.e. equation (62) in the text. Here shows the case with  $\alpha = 1.2$  and  $\mu_s = 1$ . The horizontal axis is  $x$ , which labels the position in the lens plane; the vertical axis is  $y$ , which labels the position in the source plane. The points  $(x_{\text{cr}}, -y_{\text{cr}})$  and  $(-x_{\text{cr}}, y_{\text{cr}})$  satisfy  $dy/dx = 0$ . The non-zero roots of  $y(x) = 0$  are  $\pm x_0$ . Three images are formed when  $|y| < y_{\text{cr}}$ , two images are formed when  $|y| = y_{\text{cr}}$ , one image is formed when  $|y| > y_{\text{cr}}$ . So, multiple images are formed when  $|y| \leq y_{\text{cr}}$ , an example is shown with the horizontal long dashed line ABC – which has three images: A, B, and C. In the paper we consider the splitting angle between the two outside images, i.e the splitting angle between A and C.

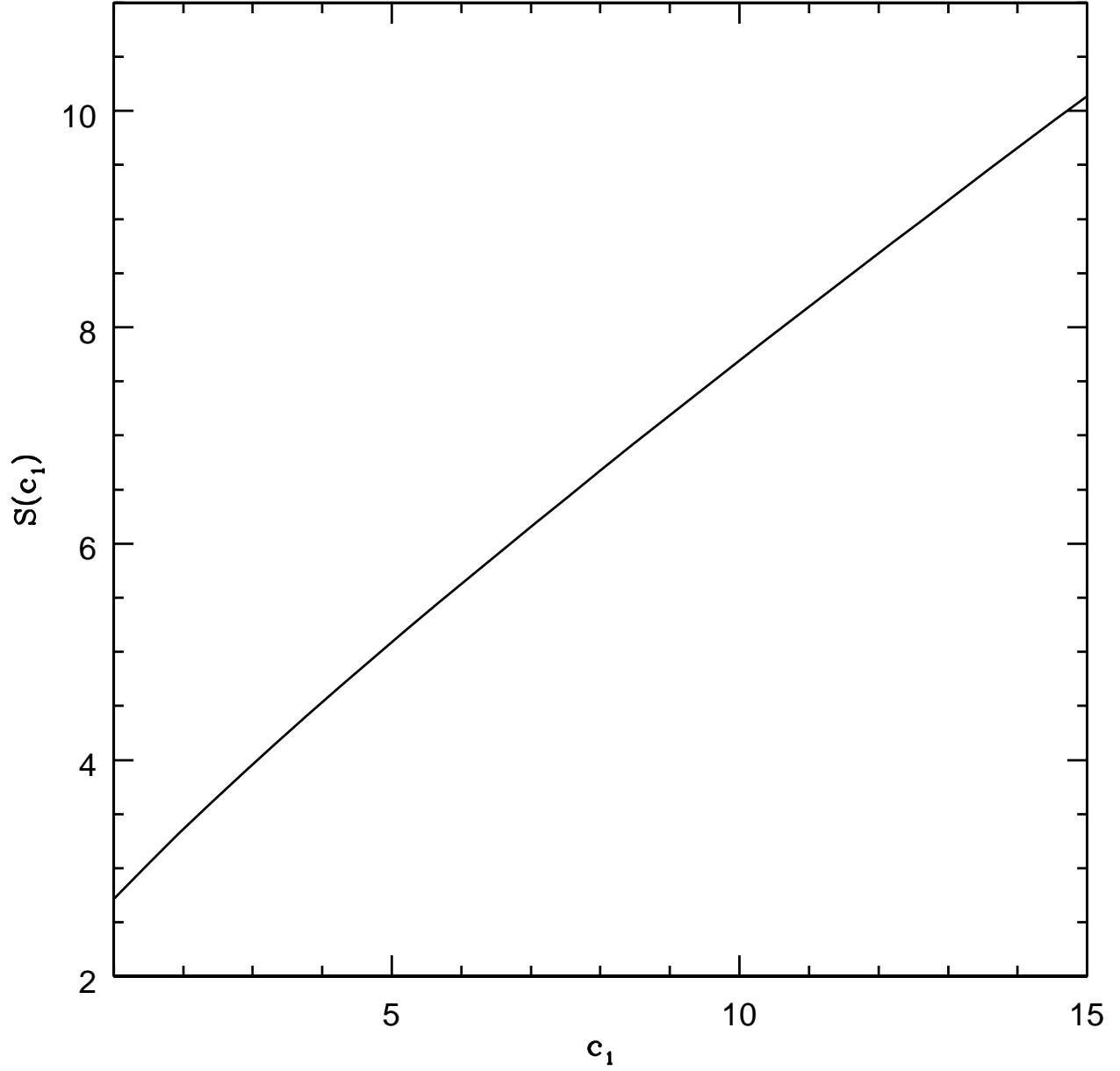


Fig. 5.—  $S(c_1) \equiv 1/\eta(c_1)^2$ , where  $c_1$  is the concentration parameter,  $\eta(c_1) \equiv r_{1/2}/r_{200}$  is determined by equation (75), where  $r_{1/2}$  is the half-mass radius of a cluster.  $S(c_1)$  is proportional to the surface mass density of a halo at the half-mass radius (eq. [79]).

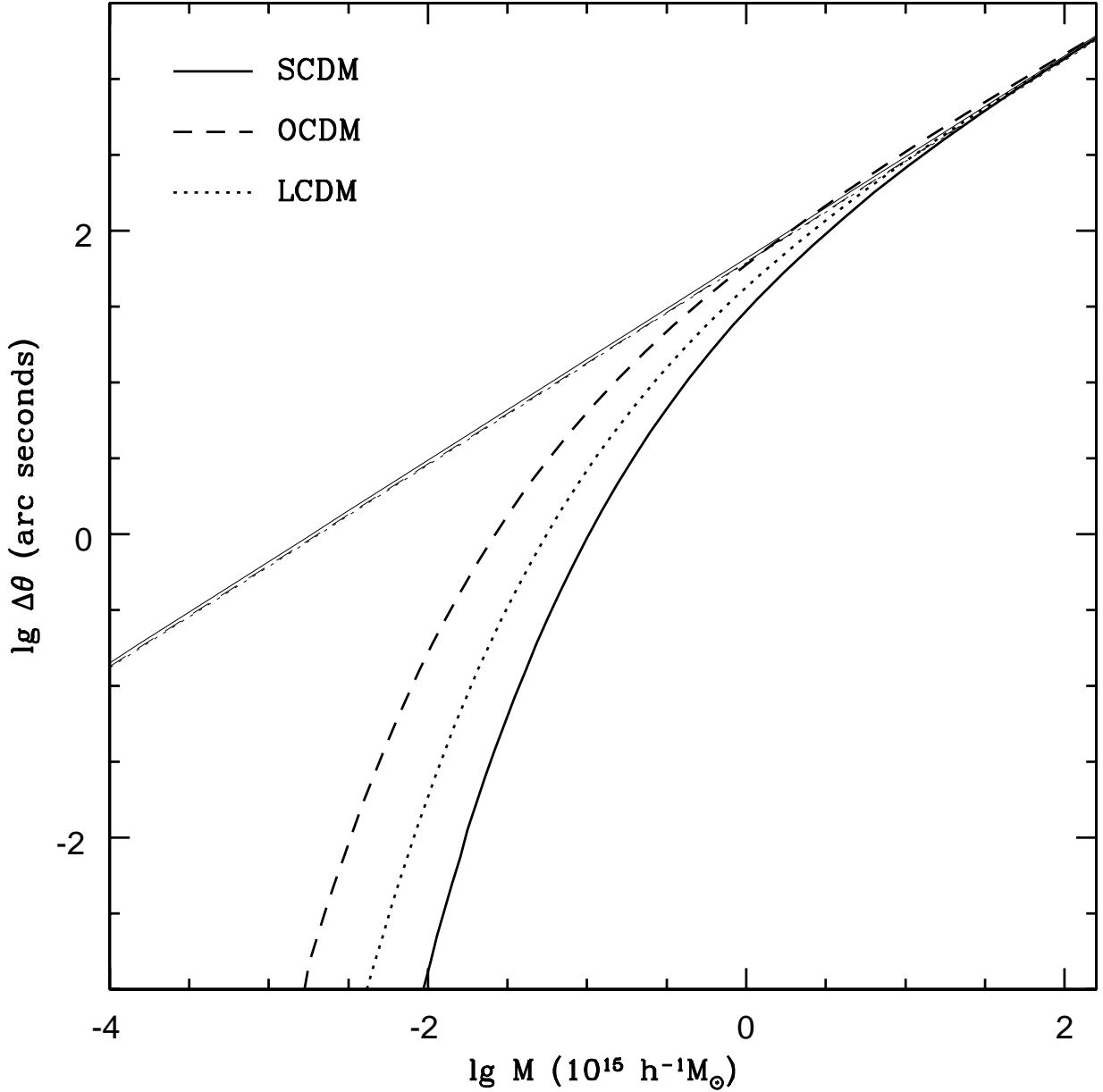


Fig. 6.— Splitting angle  $\Delta\theta$  as a function of  $M$  – the mass of the lens object. The thick lines show the splitting angle produced by a NFW lens, the thin lines show the splitting angle produced by a SIS lens. The source object is at  $z = 1.5$ , the lens object is at  $z = 0.3$ . The cosmological models are alternatively: SCDM with  $\Omega_m = 1$  (solid lines), OCDM with  $\Omega_m = 0.3$  and  $\Omega_\Lambda = 0$  (dashed lines), LCDM with  $\Omega_m = 0.3$  and  $\Omega_\Lambda = 0.7$  (dotted lines). For the NFW case, the concentration parameters are alternatively 5 for SCDM, 9 for OCDM, and 7 for LCDM. Notice the enormous sensitivity at small splittings and small (e.g. galactic) mass halos to the steepness of the inner part of the mass profile.

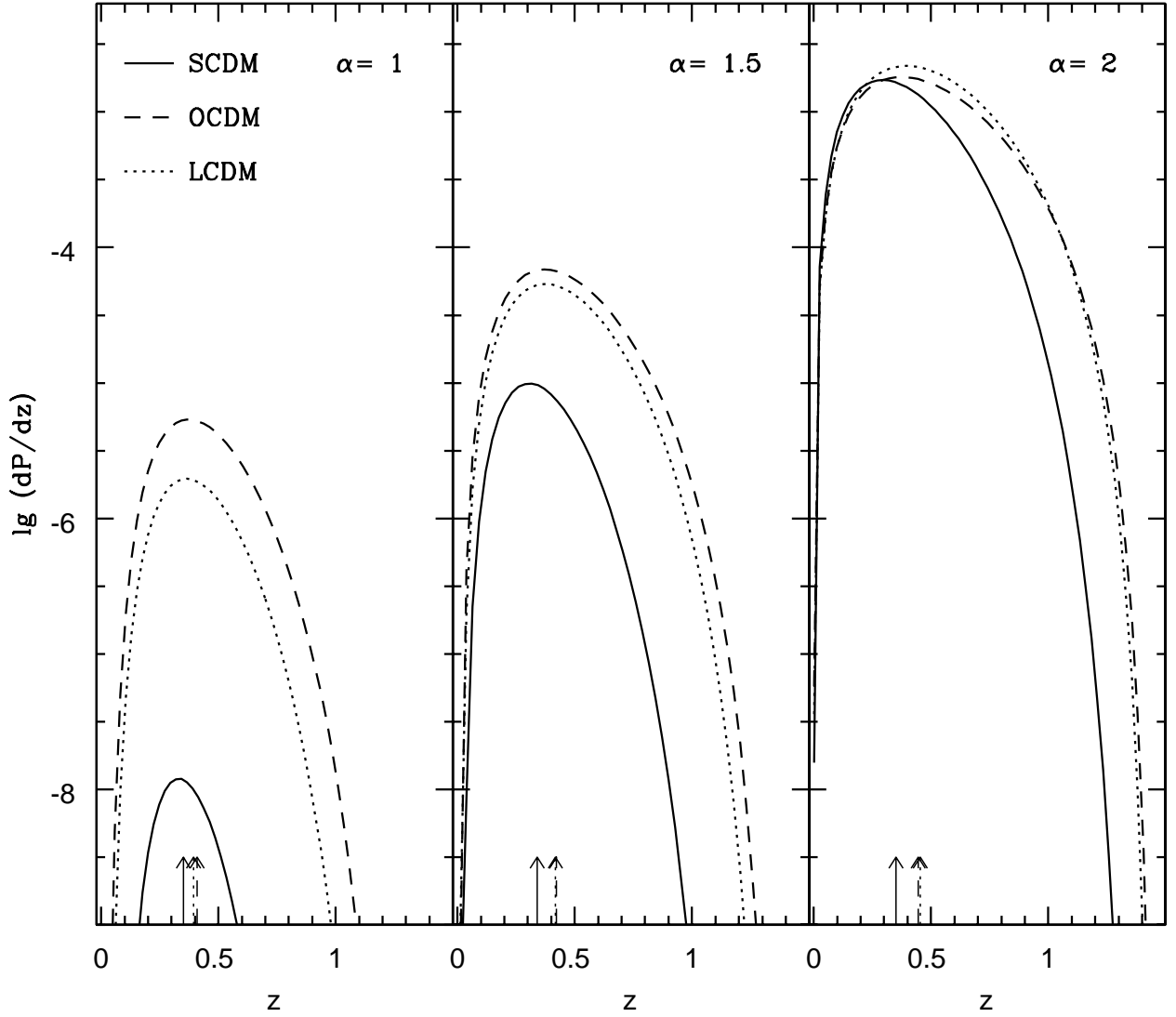


Fig. 7.— The differential lensing probability  $dP/dz$  for  $\Delta\theta > 5''$  as a function of lenses' redshift  $z$ . The source object is at  $z_s = 1.5$ . The lens objects are alternatively NFW halos (left panel, i.e. GFW halos with  $\alpha = 1$ ), GFW halos with  $\alpha = 1.5$  (central panel), and GFW halos with  $\alpha = 2$  (right panel). The concentration parameters are alternatively given by equation (76), equation (77), and equation (78). The cosmological models are alternatively: SCDM with  $\Omega_m = 1$  and  $\sigma_8 = 0.5$ ; OCDM with  $\Omega_m = 0.3$ ,  $\Omega_\Lambda = 0$ , and  $\sigma_8 = 0.85$ ; OCDM with  $\Omega_m = 0.3$ ,  $\Omega_\Lambda = 0.7$ , and  $\sigma_8 = 0.95$ . The Hubble constant is  $h = 0.7$ . The extreme sensitivity of lensing to the slope of the inner profile is evident. Arrows show median expected redshifts.

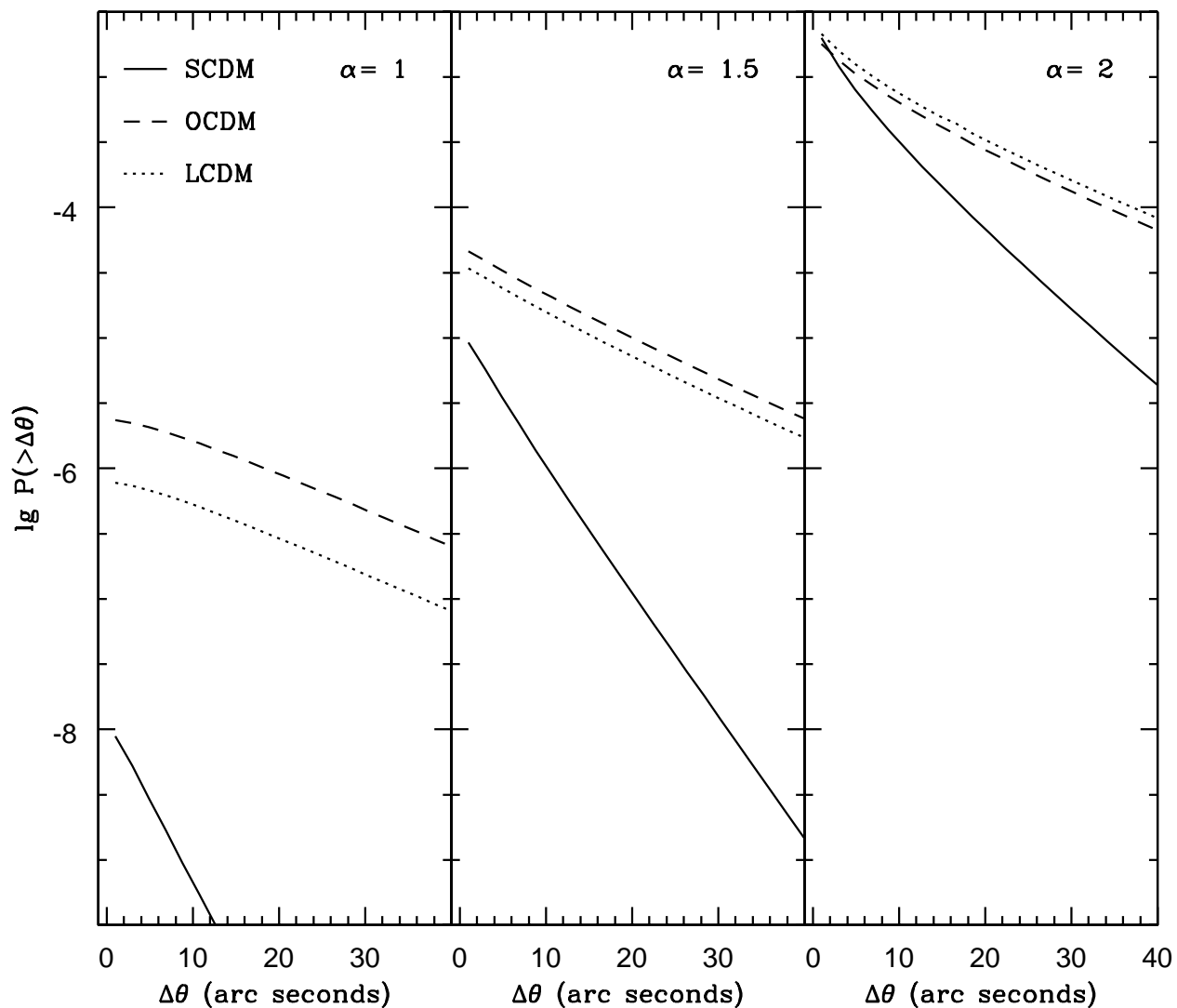


Fig. 8.— The integral lensing probability  $P(> \Delta\theta)$  as a function of  $\Delta\theta$ . The models are the same as those in Fig. 7. Note the relatively slow fall-off of probability with increasing splitting angle for the OCDM and LCDM cosmologies: for all  $\alpha$  the number of  $10''$  splittings expected is not very much smaller than the number of  $1''$  splittings expected.



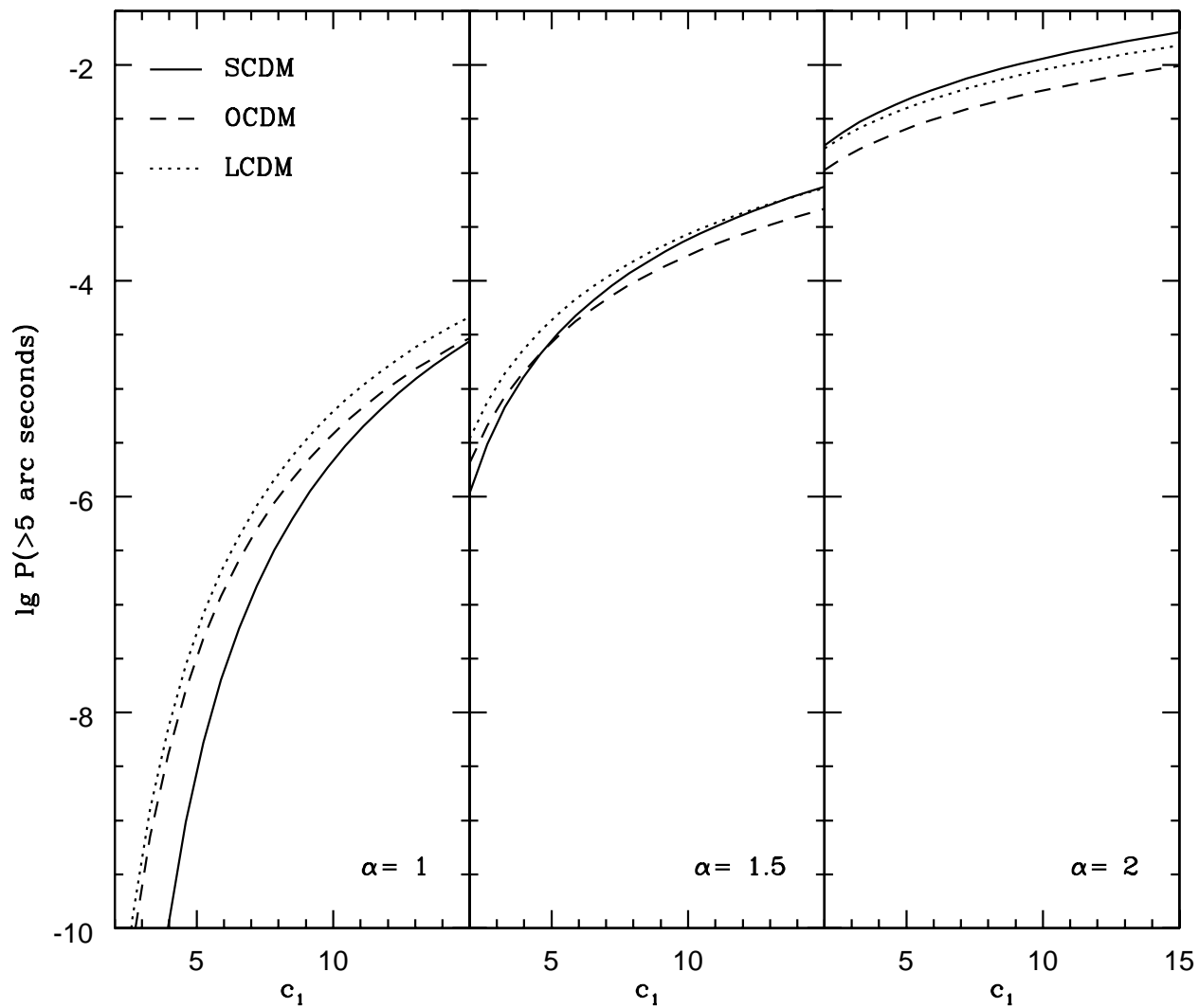


Fig. 9.— The integral lensing probability  $P(\Delta\theta > 5'')$  as a function of lenses' concentration parameter  $c_1$ . The cosmological models are the same as those in Fig. 7. The source object is at  $z_s = 1.5$ . The lens objects are alternatively NFW halos (left panel), GFW halos with  $\alpha = 1.5$  (central panel), and GFW halos with  $\alpha = 2$  (right panel).

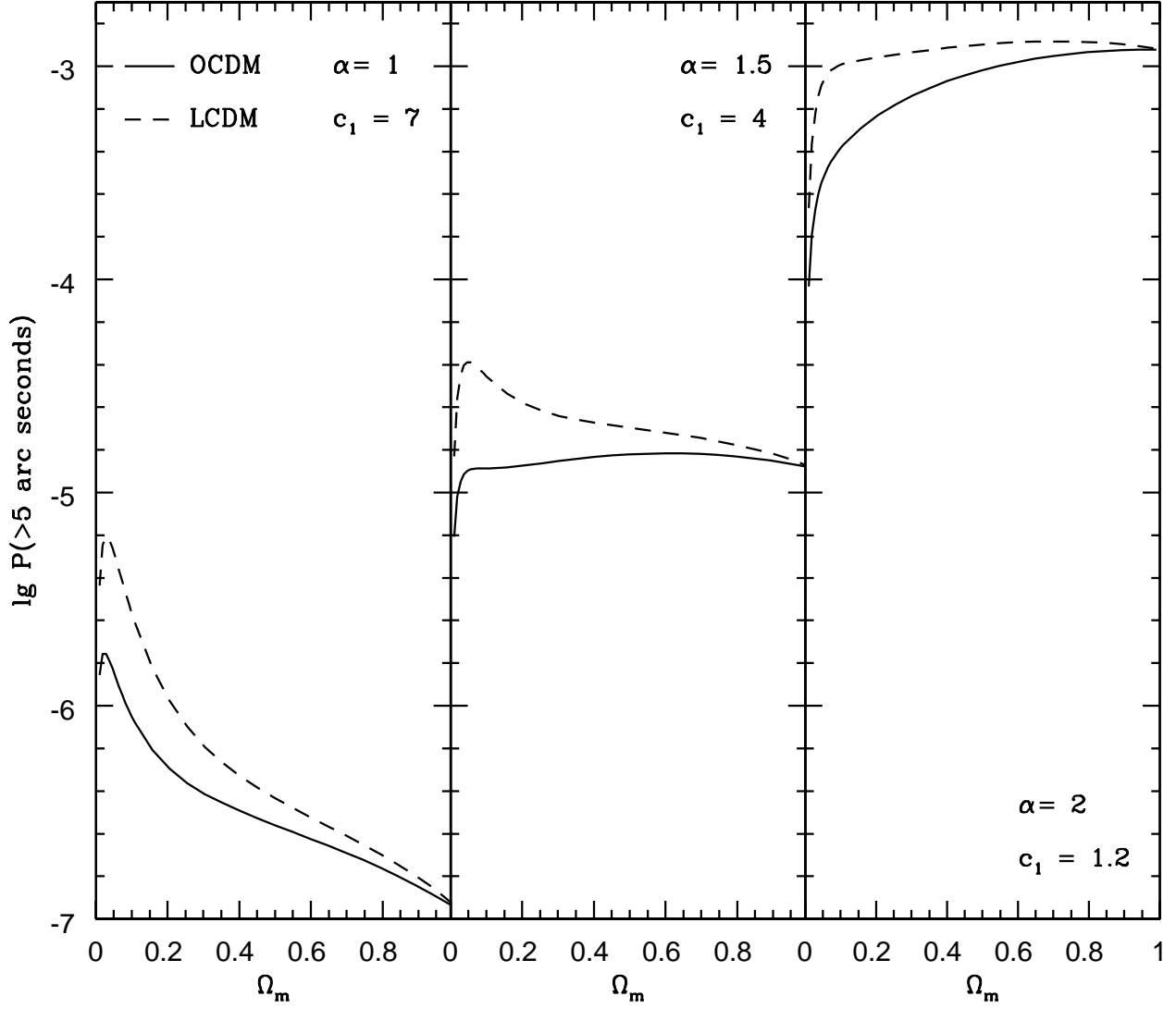


Fig. 10.— The integral lensing probability  $P(\Delta\theta > 5'')$  as a function of  $\Omega_m$  when  $\Omega_m$  and  $\sigma_8$  are constrained by equation (22). The lens models are the same as those in Fig. 7. The source object is at  $z_s = 1.5$ . The cosmological models are OCDM (solid lines) and LCDM (dashed lines). The Hubble constant is  $h = 0.7$ . Note that, for models normalized to give the correct  $z = 0$  cluster abundances, the sensitivity of the lensing probability to the halo profile shape is far stronger than to the matter density  $\Omega_m$ .

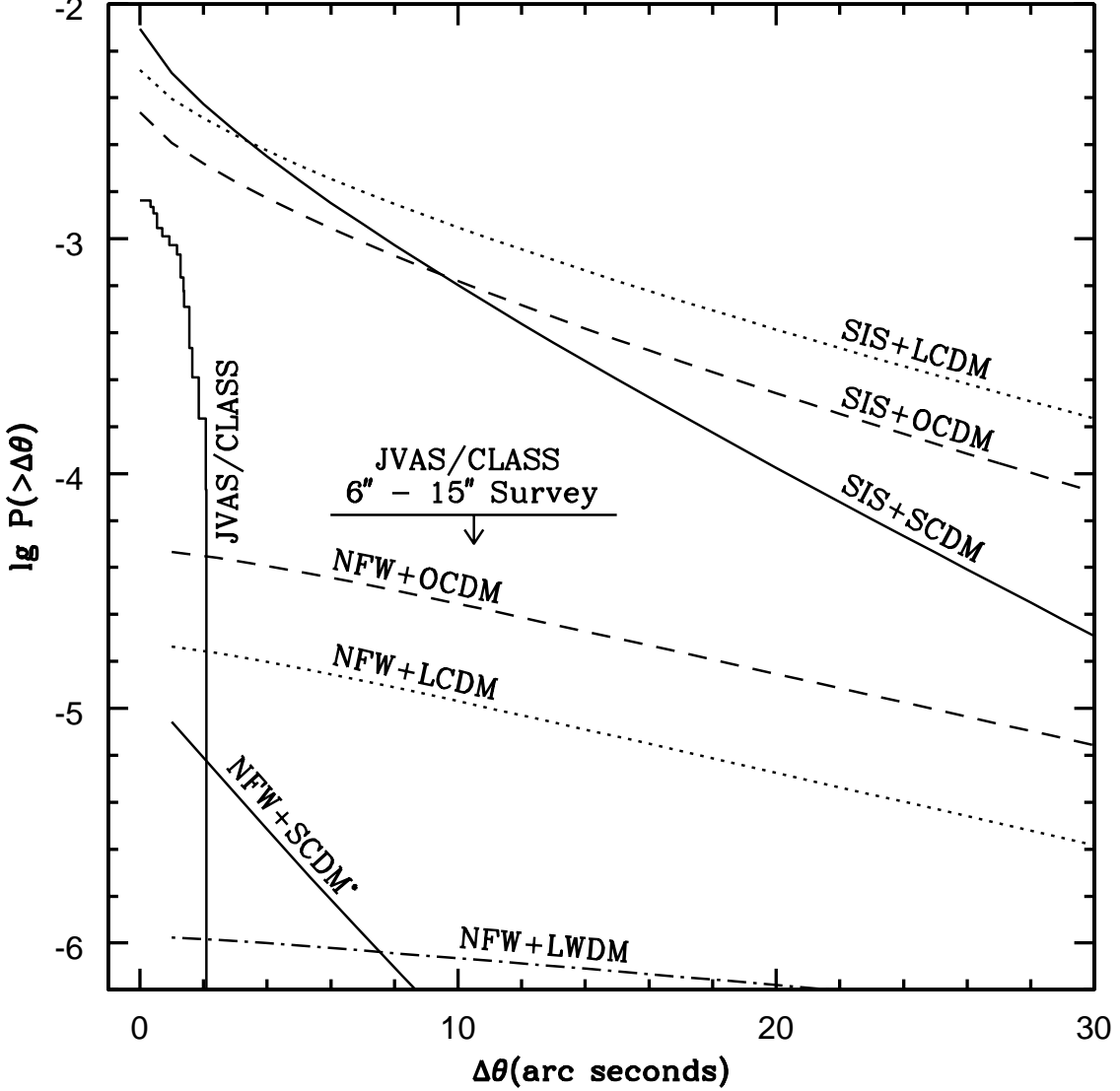


Fig. 11.— Comparison of our semi-analytical results with the JVAS/CLASS survey. The JVAS/CLASS results are shown with the histogram. The null result for lenses with  $6'' \leq \Delta\theta \leq 15''$  is shown with the horizontal line with a downward arrow indicating that is an upper limit. Our semi-analytical results (allowing for amplification bias) are shown with solid curves (SCDM with  $\Omega_m = 1$  and  $\sigma_8 = 0.5$ ), dashed curves (OCDM with  $\Omega_m = 0.3$ ,  $\Omega_\Lambda = 0$ , and  $\sigma_8 = 0.85$ ), and dotted curves (LCDM with  $\Omega_m = 0.3$ ,  $\Omega_\Lambda = 0.7$ , and  $\sigma_8 = 0.95$ ). Two groups of lenses models are shown: SIS lenses, and NFW lenses with the concentration parameter  $c_1 = 5$  for SCDM, 9 for OCDM, 7 for LCDM. The NFW+SCDM lensing probability has been multiplied by a factor  $10^{1.5}$  to fit it on the same scale as other models. For comparison we have also shown the result for a NFW+LWDM model with the dashed-dotted curve, which has the same parameters as the NFW+LCDM model except that  $c_1 = 3.5$ .

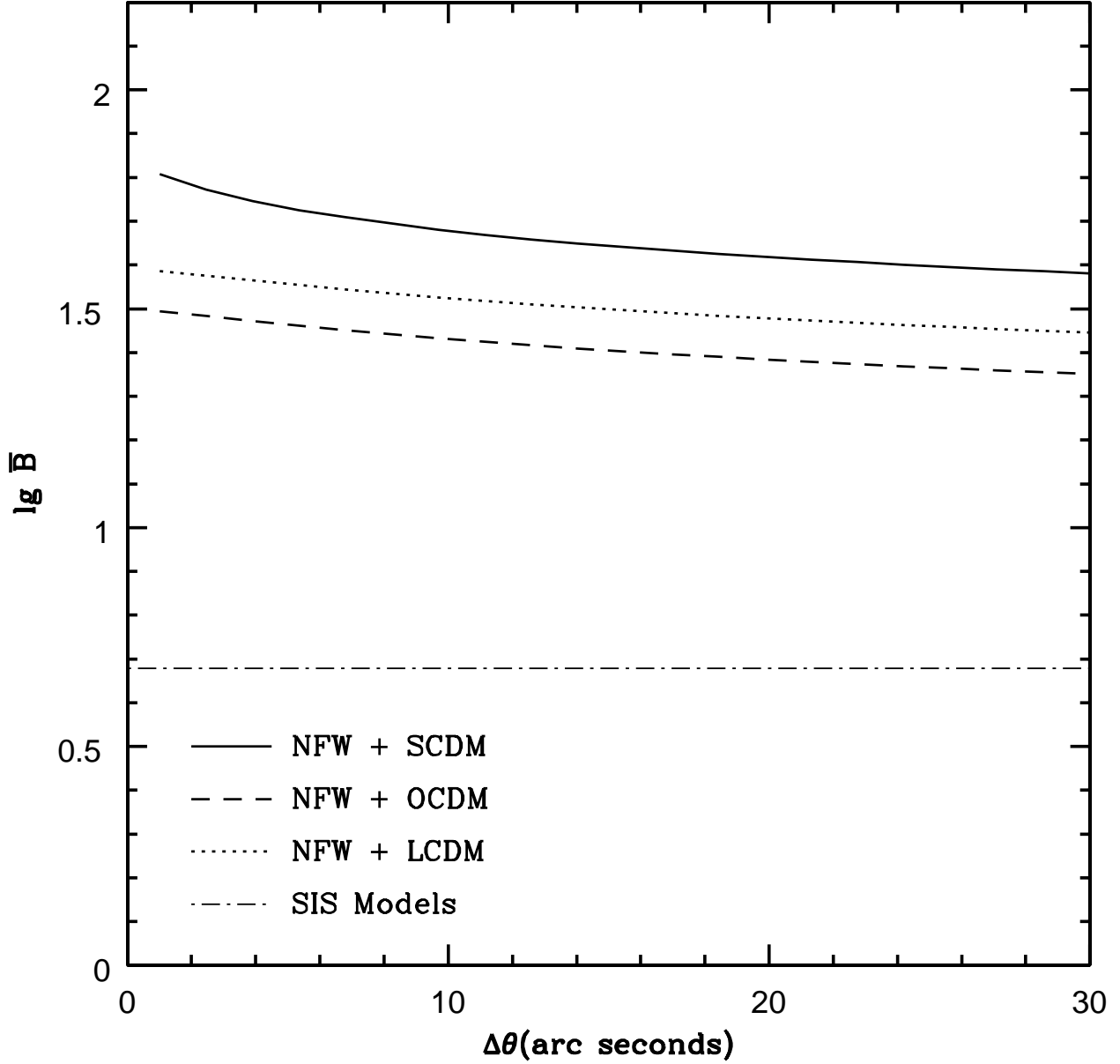


Fig. 12.— The average magnification bias as a function of splitting angles. The solid, dashed, and dotted lines are for NFW lenses, the thin dashed-dotted line is for SIS lenses. The cosmological and lens models are the same as those in Fig. 11. The magnification bias for SIS lenses is a constant independent of cosmological models.

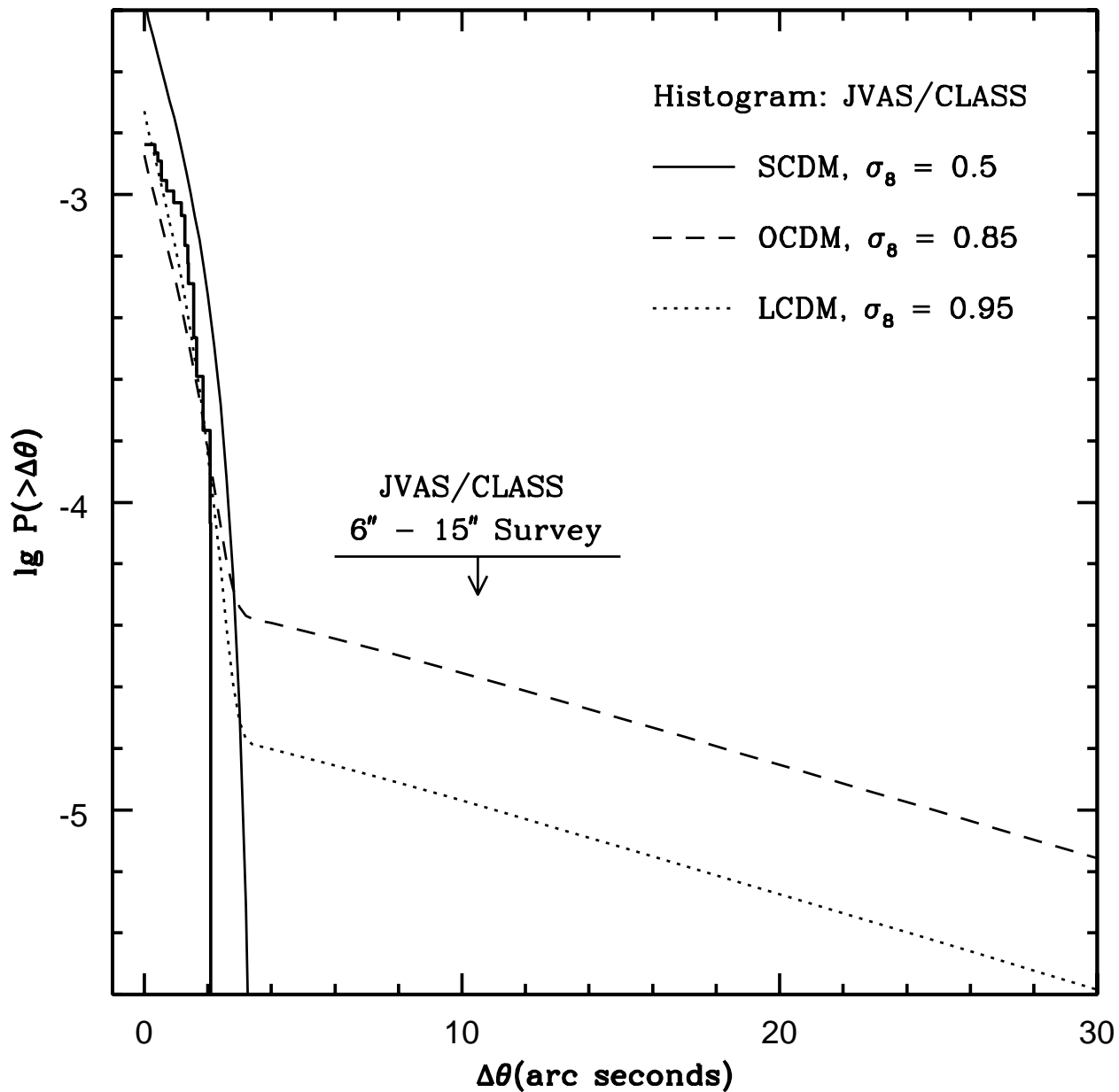


Fig. 13.— Fitting of the two-population models to the JVAS/CLASS results. The cosmological models are the same as those in Fig. 11. The lens models are: SIS halos with  $M < 10^{13} h^{-1} M_{\odot}$ , NFW halos with  $M > 10^{13} h^{-1} M_{\odot}$ . The concentration parameters for NFW halos are alternatively  $c_1 = 5$  for SCDM, 9 for OCDM, and 7 for LCDM.

Table 1. Summary of the Results for the Lensing Probability

Models	$\lg P(2'')$	$\lg P(5'')$	$\lg P(10'')$	$\lg P(20'')$	$\lg P(40'')$
SCDM <sup>a</sup> ( $\alpha = 1$ )	−8.16	−8.54	−9.17	−10.4	−12.8
SCDM <sup>a</sup> ( $\alpha = 1.5$ )	−5.14	−5.46	−5.98	−6.96	−8.84
SCDM <sup>a</sup> ( $\alpha = 2$ )	−2.82	−3.10	−3.49	−4.17	−5.36
SCDM <sup>a</sup> (SIS)	−3.00	−3.33	−3.78	−4.56	−5.97
OCDM <sup>b</sup> ( $\alpha = 1$ )	−5.64	−5.68	−5.79	−6.04	−6.60
OCDM <sup>b</sup> ( $\alpha = 1.5$ )	−4.37	−4.49	−4.66	−5.00	−5.62
OCDM <sup>b</sup> ( $\alpha = 2$ )	−2.81	−2.98	−3.20	−3.56	−4.17
OCDM <sup>b</sup> (SIS)	−3.23	−3.45	−3.74	−4.23	−5.04
LCDM <sup>c</sup> ( $\alpha = 1$ )	−6.12	−6.17	−6.28	−6.54	−7.09
LCDM <sup>c</sup> ( $\alpha = 1.5$ )	−4.50	−4.62	−4.80	−5.14	−5.77
LCDM <sup>c</sup> ( $\alpha = 2$ )	−2.74	−2.90	−3.12	−3.48	−4.08
LCDM <sup>c</sup> (SIS)	−3.04	−3.24	−3.51	−3.96	−4.69
LWDM <sup>d</sup> ( $\alpha = 1$ )	−7.45	−7.46	−7.50	−7.59	−7.80

<sup>a</sup>SCDM:  $\Omega_m = 1$ ,  $\Omega_\Lambda = 0$ ,  $\sigma_8 = 0.5$ ,  $c_1(z = 0) = 5$  for  $\alpha = 1$ .

<sup>b</sup>OCDM:  $\Omega_m = 0.3$ ,  $\Omega_\Lambda = 0$ ,  $\sigma_8 = 0.85$ ,  $c_1(z = 0) = 9$  for  $\alpha = 1$ .

<sup>c</sup>LCDM:  $\Omega_m = 0.3$ ,  $\Omega_\Lambda = 0.7$ ,  $\sigma_8 = 0.95$ ,  $c_1(z = 0) = 7$  for  $\alpha = 1$ .

<sup>d</sup>LWDM:  $\Omega_m = 0.3$ ,  $\Omega_\Lambda = 0.7$ ,  $\sigma_8 = 0.95$ ,  $c_1(z = 0) = 3.5$  for  $\alpha = 1$ .

Note. — The GFW parameter  $\alpha$  is defined in equation (60). SIS = singular isothermal sphere. The source object is at  $z_s = 1.5$ . The Hubble constant is  $h = 0.7$ . The magnification bias is not included, so  $P(\Delta\theta) = P(> \Delta\theta)$  is the intrinsic lensing probability.